Membrane Contact Sites Between Chloroplasts and Pathogen Interface Underpin Plant Focal Immune Responses

Enoch Lok Him Yuen[1], Zachary Savage[1], Vanda Adamkova[1], Cristina Vuolo[1], Yuanyang Zhou[1], Yasin Tumtas[1], Jessica Lee Erickson[2], Jennifer Prautsch[3], Andrada I. Balmez[1], Johannes Stuttmann[4,5], Cian Duggan[1], Francesco Rivetti[1], Camilla Molinari[1], Martin Schattat[3,*], Tolga O. Bozkurt[1,*]

Affiliation

[1]: Department of Life Sciences, Imperial College London, London SW7 2AZ, UK.

[2]: Department of Biochemistry of Plant Interactions, Leibniz Institute for Plant Biochemistry, Weinbergweg 10, Halle 06120, Germany.

[3]: Department of Plant Physiology, Martin-Luther-University Halle-Wittenberg, Weinbergweg 10, Halle 06120, Germany.

[4]: Department of Plant Genetics, Martin-Luther-University Halle-Wittenberg, Weinbergweg 10, Halle 06120, Germany.

[5]: Aix Marseille University, CEA, CNRS, BIAM, UMR7265, LEMiRE (Microbial Ecology of the Rhizosphere), 13115, Saint-Paul lez Durance, France.

*Correspondence: martin.schattat@pflanzenphys.uni-halle.de (M. S.), o.bozkurt@imperial.ac.uk (T.O.B.)

Twitter handles: @EnochYuen, @Tolga_Bzkrt

Abstract

Communication between cellular organelles is essential for mounting effective innate immune responses to eliminate pathogens. In plants, the transport of cellular organelles to pathogen penetration sites and their assembly around the host membrane delineating plant-pathogen interface are well-documented. However, whether organelles associate with these specialized plant-pathogen membrane interfaces and the extent to which this process contributes to immunity remain unknown. Here, we discovered defense-related membrane contact sites (MCS) comprising a membrane tethering complex between chloroplasts and the extrahaustorial membrane (EHM) surrounding the pathogen haustorium. The assembly of this membrane tethering complex relies on the association between the chloroplast outer envelope protein CHLOROPLAST UNUSUAL POSITIONING 1 (CHUP1), and its plasma membrane-associated partner, KINESIN-LIKE PROTEIN FOR ACTIN-BASED CHLOROPLAST MOVEMENT 1 (KAC1). Our biochemical assays revealed that CHUP1 and KAC1 interact, while infection cell biology demonstrated their co-accumulation in foci where chloroplasts contact the EHM. Genetic depletion of CHUP1 or KAC1 reduces the deposition of callose—a cell wall material typically deployed to fortify pathogen penetration resistance—around the haustorium, without affecting other core immune processes. Our findings suggest that the chloroplast-EHM attachment complex positively regulates plant focal immunity, revealing the key components and their potential roles in the targeted deposition of defense components at the pathogen interface. These results advance our understanding of organelle-mediated immune responses and highlight the significance of MCS in plant-pathogen interactions.

47 **Introduction**

48 Filamentous pathogens such as oomycetes and fungi intimately interact with plant hosts, often
49 through specialized infection structures that penetrate the host cells. In response, the invaded plant
50 cell activates a cell-autonomous defense mechanism interface known as focal immunity[1-4]. This
51 defense involves significant cellular reorganization, including organelle relocation, cell-wall
52 reinforcements at pathogen contact sites via callose deposition, and the polarized secretion of
53 antimicrobials[3,5-7]. In addition to the secretory system and the nucleus, organelles such as
54 chloroplasts, mitochondria and peroxisomes accumulate around host cell penetration sites of
55 fungal and oomycete pathogens[5,7,8]. However, the physical association of organelles with the plant-
56 pathogen interface and the extent to which these processes contribute to immunity remain unclear.

57 Cellular homeostasis relies on efficient interorganelle communication, a process facilitated by
58 long-range vesicle trafficking and short-range membrane contact sites (MCS). MCS are
59 specialized regions where organelles come into close proximity, allowing for the direct transfer of
60 lipids, proteins, signaling molecules, and metabolites. These sites serve as critical gateways for
61 rapid and effective intracellular communication, enabling cells to quickly adapt and respond to
62 stress conditions[9-11]. Recent research has highlighted the emerging roles of MCS in mammalian
63 innate immunity[12]. Moreover, pathogens have developed strategies to target and subvert MCS,
64 perturbing interorganelle communications to undermine host immune defenses and exploit cellular
65 resources[13,14]. However, the involvement of MCS in plant-pathogen interactions remains
66 unexplored. Additionally, the identity and roles of protein-tethering complexes that regulate the
67 functions of MCS in plants are still largely elusive[11]. Understanding these mechanisms could
68 reveal new insights into how organelle communication contributes to immune responses.

69 Accumulating evidence points to key roles of chloroplasts in the deployment of various plant
70 immune responses[15,16]. Upon immune activation and signaling mediated through mitogen-
71 activated protein kinases (MAPKs), chloroplasts terminate photosynthesis and activate a range of
72 defense responses such as the production of reactive oxygen species (ROS) and defense
73 hormones[17]. During the immune response, chloroplasts alter their morphology by extending
74 stroma-filled tubules, called stromules, that can make contacts with other membranes and
75 organelles such as the nucleus[7,18,19]. In addition, chloroplasts cluster around the nucleus during
76 immune stimulation[20], a response that is presumed to contribute towards plant defense, possibly
77 through facilitating more efficient chloroplast-to-nucleus signaling. Consistent with the emerging
78 roles of chloroplast in immunity, an increasing number of effectors secreted by pathogens have
79 been found to target chloroplast functions, whereas plants monitor these potential threats using
80 nucleotide-binding leucine-rich repeat (NLR) immune receptors[21-27].

81 The Irish potato famine pathogen, *Phytophthora infestans*, can penetrate host cells via specialized
82 infection structures called haustoria, which mediate the delivery of effector proteins inside the host
83 cells. Haustoria are excluded from the host cytoplasm through a newly synthesized plant-derived
84 membrane called the extrahaustorial membrane (EHM)[28-30]. Remarkably, chloroplasts frequently
85 gather around *P. infestans* haustoria and appear to establish tight contacts with the EHM[7]. Given
86 the range of antimicrobial and defense components produced by chloroplasts, their positioning at
87 the pathogen interface likely contributes to focal plant immune responses. The mechanisms
88 underlying chloroplast photorelocation in response to light intensity, involving membrane
89 attachment, detachment, and movement, are relatively well understood, with key components such
90 as CHLOROPLAST UNUSUAL POSITIONING 1 (CHUP1) and KINESIN-LIKE PROTEIN
91 FOR ACTIN-BASED CHLOROPLAST MOVEMENT 1 (KAC1) identified[31-34]. Both CHUP1

92 and KAC1 are involved in the photorelocation movement of chloroplasts and the association of
93 chloroplasts with the plasma membrane (PM) by regulating short actin filaments on the chloroplast
94 envelope (cp-actin filaments)[31,32,34,35]. However, the extent to which chloroplast movement and
95 positioning around the haustoria contributes to plant immunity remains to be elucidated.

96 In this study, we investigated the role of the chloroplast movement and membrane anchoring
97 protein CHUP1 in plant immunity against *P. infestans*. Using virus-induced gene silencing (VIGS)
98 and CRISPR knockouts, we found that CHUP1-deficient *N. benthamiana* plants exhibit
99 significantly increased pathogen growth, indicating that CHUP1 positively contributes to
100 immunity. Despite no significant changes in chloroplast movement towards haustoria or other core
101 immune processes such as MAPK-triggered signaling and hypersensitive response (HR) cell death,
102 CHUP1-knockout plants showed reduced callose deposition at haustoria penetration sites,
103 highlighting the involvement of CHUP1 in focal immune responses. We discovered that CHUP1
104 interacts with the kinesin-like protein KAC1, and both proteins co-accumulate at chloroplast-EHM
105 MCS. This suggests their cooperative role in anchoring chloroplasts to the pathogen interface and
106 enhancing immunity. Consistently, KAC1 accumulated at chloroplast-EHM MCS in a CHUP1-
107 dependent manner, and depletion of KAC1 led to reduced callose deposition around the
108 haustorium and enhanced disease susceptibility. These findings underscore the importance of
109 CHUP1 and KAC1 cooperation in coordinating the tethering of chloroplasts to the pathogen
110 interface and mounting effective immune responses via MCS.

111

112

113

114 **Results**

115

116 **CHUP1 positively contributes to immunity against *Phytophthora infestans***

117 The role of chloroplasts in providing biochemical defense against pathogens is well
118 established[15,16,18]. An emerging yet less understood aspect of chloroplast immunity involves the
119 positioning and movement of epidermal chloroplasts during infection and their contribution to the
120 immune response[20,36]. We previously demonstrated that during infection by the oomycete
121 pathogen *Phytophthora infestans*, epidermal chloroplasts in the model solanaceous plant *Nicotiana*
122 *benthamiana* accumulate around the haustoria[7]. To investigate this phenomenon further, we
123 performed infection assays on *N. benthamiana* following the downregulation of the chloroplast
124 movement and anchoring gene, *CHUP1*. Silencing the two identified *CHUP1* alleles (*NbCHUP1a*
125 and *NbCHUP1b*) in transgenic *N. benthamiana* expressing GFP in the chloroplast stroma (CP
126 plants) via virus-induced gene silencing (VIGS) (Figure S1A) resulted in significantly higher
127 levels of hyphal growth of tdTomato-expressing *P. infestans* compared to the silencing control
128 (Figures S1B and S1C). To further validate these findings, we generated CRISPR knockout lines
129 lacking *NbCHUP1a* and *NbCHUP1b* (referred to as *chup1* KO plants) from a transgenic parental
130 line of *N. benthamiana* expressing the chimeric protein FNR:eGFP, which targets the plastid
131 stroma (referred to as FNR plants) (Figure S1D). *chup1* KO plants did not exhibit any major
132 developmental defects compared to FNR control plants (Figure S1E). Following infection with *P.*
133 *infestans*, the mean hyphal growth of the pathogen was approximately 3.3-fold higher in *chup1*
134 KO plants compared to FNR control plants (Figures 1A and 1B), indicating that *chup1* KO plants
135 are significantly more susceptible than the FNR control plants. Additionally, we generated
136 independent *chup1* knockout lines from wild-type (WT) *N. benthamiana* plants (Figure S1F)

137 (referred to as *chup1* KO#2 plants). These *chup1* KO#2 plants also demonstrated significantly
138 higher *P. infestans* hyphal growth compared to the WT control plants (Figures 1C and 1D). These
139 results implicate that the chloroplast outer envelope protein CHUP1 contributes to plant defense
140 against adapted pathogens.

141 CHUP1 is known to facilitate chloroplast movement and photorelocation through cp-actin
142 polymerization[31,37,38]. Therefore, we hypothesized that increased susceptibility in *chup1* KO plants
143 could be due to perturbations in chloroplast movement and positioning around the haustoria. To
144 investigate this, we imaged infected *N. benthamiana* epidermal cells and quantified chloroplast-
145 haustoria associations in *chup1* KO and FNR plants. Our quantitative analysis showed no
146 significant difference in the number of haustoria that is associated with chloroplasts between *chup1*
147 KO and FNR plants (Figures S1G and S1H), indicating that enhanced susceptibility upon loss of
148 CHUP1 is not due to impaired chloroplast movement towards the haustoria.

149 Chloroplasts clustering around nucleus is regarded to be a general plant immune response upon
150 pathogen recognition and immune activation[18,20]. Therefore, we next checked whether chloroplast
151 accumulation around the haustoria is impaired in *chup1* KO plants. Intriguingly, microscopy
152 analysis revealed that chloroplasts tend to accumulate more around the nucleus in *chup1* KO plants
153 compared to FNR plants (Figures S1I and S1J), indicating that the enhanced susceptibility of *chup1*
154 KO plants is not due to impaired perinuclear clustering of chloroplasts. Lastly, we revealed that
155 the number of chloroplasts in the epidermal cells and the total chlorophyll concentration in leaves
156 did not vary significantly between *chup1* KO and FNR plants (Figures S1K-M). Altogether, these
157 results indicate that CHUP1 is not essential for chloroplast positioning around haustoria, and the
158 increased disease susceptibility in CHUP1 knockouts is not due to impaired chloroplast positioning
159 or abnormal chloroplast numbers.

160

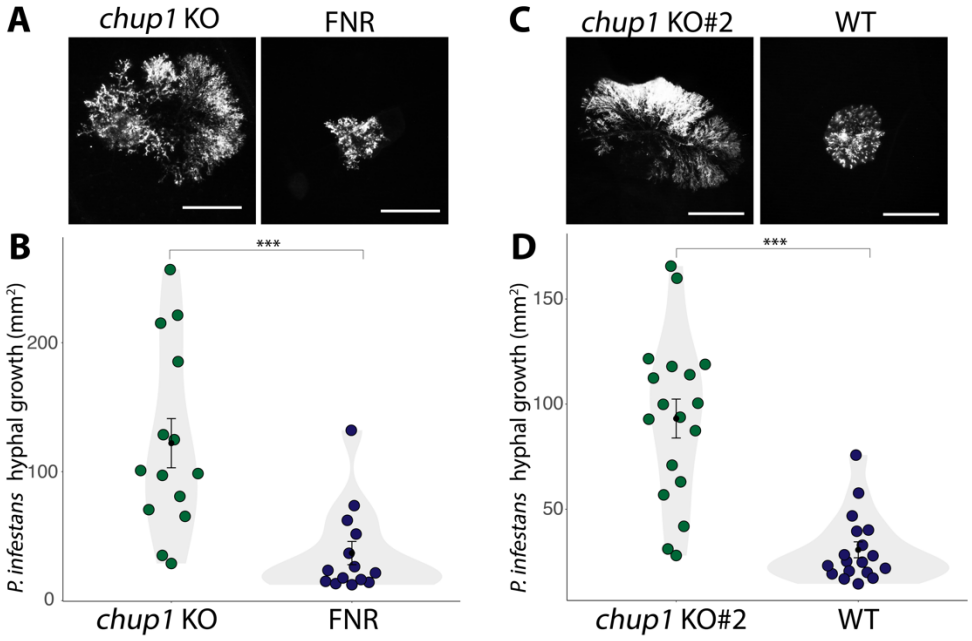

161

162 **Figure 1. CHUP1 positively contributes to immunity against *P. infestans*.** (A-B) *chup1* KO
163 plants increase hyphal growth of *P. infestans* compared to control FNR plants. (A) 4-week-old
164 *chup1* KO and FNR leaves were infected with tdTomato-expressing *P. infestans*, and pathogen
165 growth was calculated by measuring hyphal growth using fluorescence stereomicroscope at 5 days
166 post-inoculation. Scale bars represent 5 mm. (B) Violin plot illustrating that *chup1* KO plants
167 (122.1 mm^2, n = 83 infection spots) display a significant increase in *P. infestans* hyphal growth
168 compared to control FNR plants (36.9 mm^2, n = 83 infection spots). (C-D) *chup1* KO#2 plants
169 increase hyphal growth of *P. infestans* compared to control WT plants. (C) 4-week-old *chup1*
170 KO#2 and WT leaves were infected with tdTomato-expressing *P. infestans*, and pathogen growth
171 was calculated by measuring hyphal growth using fluorescence stereomicroscope at 5 days post-
172 inoculation. Scale bars represent 5 mm. (D) Violin plot illustrating that *chup1* KO#2 plants (93.1
173 mm^2, n = 97 infection spots) exhibit a significant increase in *P. infestans* hyphal growth compared

174 to control FNR plants (30.7 mm^2, n = 94 infection spots). Each dot represents the average of all
175 infection spots on the same leaf, with each leaf having between 3 to 6 infection spots. Statistical
176 differences were analyzed by Mann-Whitney U test in R. Differences in measurements were
177 considered highly significant when $p<0.001$ (***).
178

179 **CHUP1 accumulates at the chloroplast-plasma membrane and chloroplast-extrahaustorial**
180 **membrane contact sites**

181 To build on our findings of enhanced susceptibility in *chup1* KO plants, we next explored the cell
182 biology of CHUP1 to better understand its role. We generated a C-terminal green fluorescent
183 protein (GFP) fusion of CHUP1 (CHUP1:GFP) and examined its cellular localization using
184 confocal microscopy. By co-expressing CHUP1:GFP with the PM marker REMORIN1.3
185 (REM1.3) tagged with red fluorescent protein (RFP), we observed that CHUP1:GFP accumulates
186 at the chloroplast-PM membrane contact sites (MCS), forming puncta at this interface (Figure 2A).
187 To validate this observation, we used Toc64:GFP as a control since both CHUP1 and Toc64 are
188 chloroplast outer membrane proteins[39]. Unlike CHUP1:GFP, Toc64:GFP uniformly labeled the
189 chloroplast outer membrane without forming punctate accumulations at chloroplast-PM MCS
190 (Figure 2B). This contrast highlights the specific punctate localization pattern of CHUP1 at
191 chloroplast-PM MCS.

192 Compared to the PM, the EHM has different lipid and protein contents, with most typical
193 membrane proteins excluded from it[5,40,41]. Therefore, we next examined the localization of
194 CHUP1, focusing on potential chloroplast-extrahaustorial membrane (EHM) MCS, in the context
195 of *P. infestans* infection. Our live cell imaging of infected plant cells revealed that CHUP1:GFP
196 also accumulates at foci where chloroplasts make contacts with the EHM (Figures 2C and S2A).

197 In contrast, Toc64:GFP, used as a control, continued to show uniform labeling of the chloroplast
198 outer membrane without any punctate accumulations at chloroplast-EHM MCS (Figures 2D and
199 S2B). These observations reveal the distinctive accumulation of CHUP1 at MCS, both at
200 chloroplast-PM and chloroplast-EHM, pointing to a role in chloroplast attachment to the pathogen
201 interface.

202

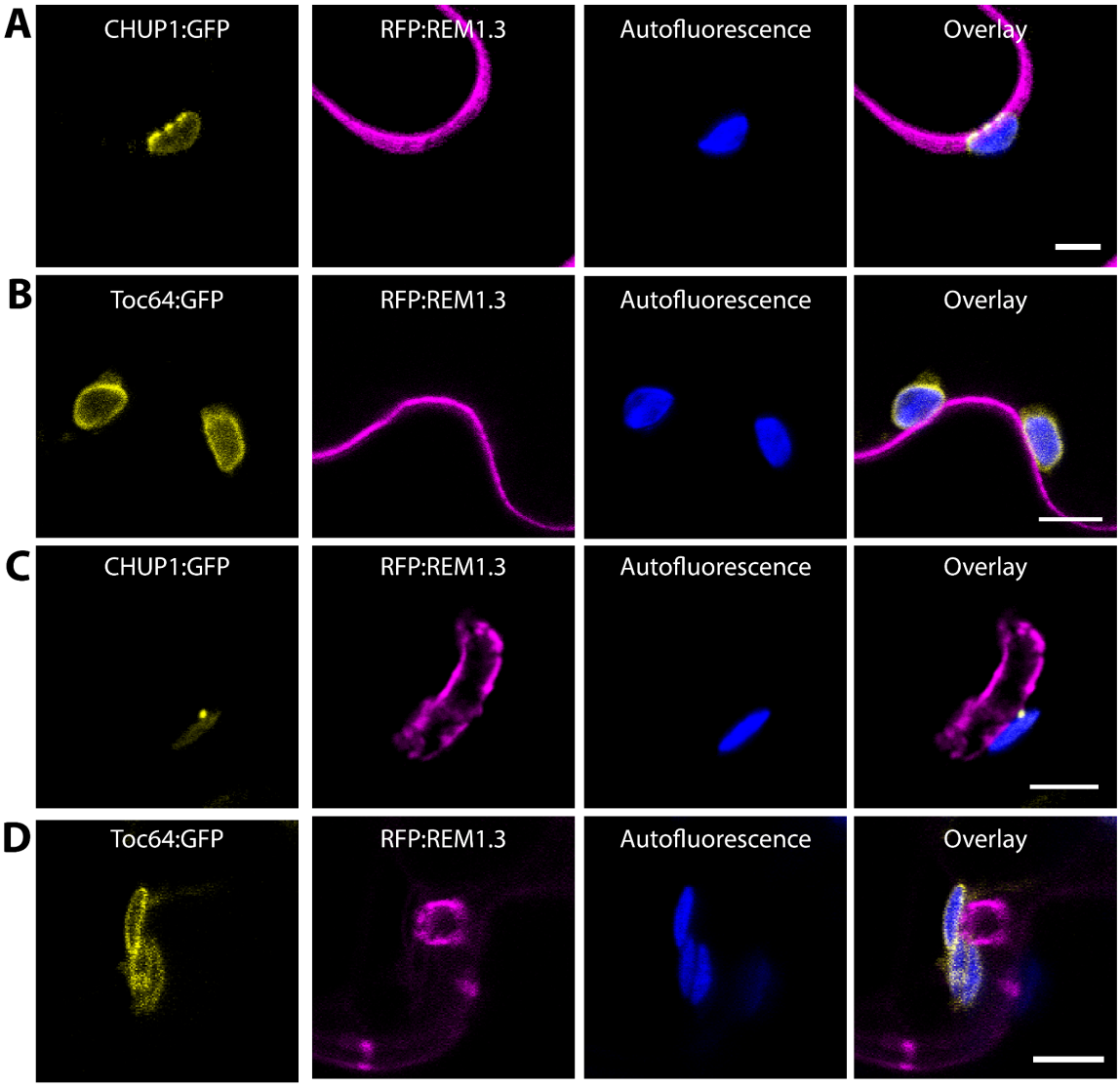

203

204 **Figure 2. CHUP1 forms punctate accumulation at chloroplast-PM and chloroplast-EHM**
205 **membrane contact sites (MCS)**. (A-B) CHUP1 forms punctate accumulation at chloroplast-PM
206 MCS, but the control Toc64 does not. Confocal micrographs of *N. benthamiana* leaf epidermal
207 cells transiently expressing either (A) CHUP1:GFP, or (B) Toc64:GFP, with RFP:REM1.3.
208 Images were taken at 3 dpi. (C-D) CHUP1 forms punctate accumulation at chloroplast-EHM MCS,
209 but the control Toc64 does not. Confocal micrographs of *N. benthamiana* leaf epidermal cells
210 transiently expressing either (C) CHUP1:GFP, or (D) Toc64:GFP, with RFP:REM1.3. The leaves
211 were infected with WT *P. infestans* spores at 6 hpi. Images were taken at 3 dpi. REM1.3 is used
212 as a PM and EHM marker. Presented images are single plane images. Scale bars represent 5 µm.
213

214 **CHUP1 contributes to callose deposition at haustorium penetration sites**

215 Recognizing that the increased disease susceptibility in *chup1* KO plants is not due to impaired
216 chloroplast positioning around haustoria or abnormal chloroplast numbers (Figures S1G, S1H,
217 S1K-M), and given that CHUP1 appears to anchor chloroplasts to the EHM (Figure 2C), we
218 investigated whether focal plant immune responses towards the pathogen are altered in *chup1* KO
219 plants. Accumulation of beta-glucan callose at haustoria penetration sites is a well-established
220 focal immune response typically observed during plant invasion by fungal and oomycete
221 pathogens[3,5,41]. To determine if callose deposition at the haustorium neck is affected in the absence
222 of CHUP1, we employed aniline blue staining to visualize callose deposition around *P. infestans*
223 haustorium in *chup1* KO and FNR plants (Figure 3A). Consistent with previous findings on
224 accumulation of callose at the neckband of *P. infestans* haustoria[42], approximately 20.4% of
225 haustoria in infected FNR plants exhibited focal callose deposits (Figure 3B). Notably, we
226 observed a 47.1% reduction in the number of haustoria with a callose neckband band in *chup1* KO

227 plants, with only 10.8% of haustoria showing callose staining (Figure 3B). These results indicate
228 that CHUP1 is implicated in focal callose deposition at the haustoria of *P. infestans*.
229 We then investigated whether other core immune pathways were disrupted in *chup1* KO plants.
230 To determine if basal immune responses following pathogen-associated molecular pattern (PAMP)
231 recognition are altered in the absence of CHUP1, we measured mitogen-activated protein kinase
232 (MAPK) phosphorylation after infiltrating leaves with *Phytophthora infestans* (Pi) extract[3], which
233 serves as a PAMP. Both *chup1* KO and FNR control plants showed a comparable increase in
234 MAPK phosphorylation 24 hours post-PAMP treatment (Figure S3A). Next, we examined whether
235 late-stage immune responses, such as defense-related cell death activation, were impaired in *chup1*
236 KO plants. Following the expression of an autoactive variant of a MEK2-like NbMAPKK
237 ($MEK2^{DD}$)[43], both *chup1* KO and FNR plants displayed a full tissue necrosis phenotype compared
238 to the EV control (Figures S3B and S3C). We also tested whether effector-triggered immunity was
239 impaired in the absence of CHUP1. To assess this, we co-expressed three cell death elicitors with
240 their cognate NLR receptors in plants: *P. infestans* AVR3a with receptor R3a[44], *P. infestans*
241 effector AVRblb2 with receptor Rpi-blb2[45], and potato virus X coat protein (PVX-CP) with
242 receptor Rx[46]. Our cell death analysis showed that both *chup1* KO and FNR plants induced cell
243 death to similar degrees in responses to AVR3a and R3a (Figures S3D and S3E), AVRblb2 and
244 Rpi-blb2 (Figures S3F and S3G), and PVX-CP and Rx (Figures S3H and S3I). Altogether, these
245 findings demonstrate that the activation of PAMP- or effector-triggered immunity is not impaired
246 in the absence of CHUP1. We conclude that the enhanced susceptibility of *chup1* KO plants is
247 most likely due to perturbations of MCS between chloroplasts and the EHM, leading to impaired
248 focal immune responses as indicated by the reduced focal deployment of callose at the haustorium
249 interface.

250

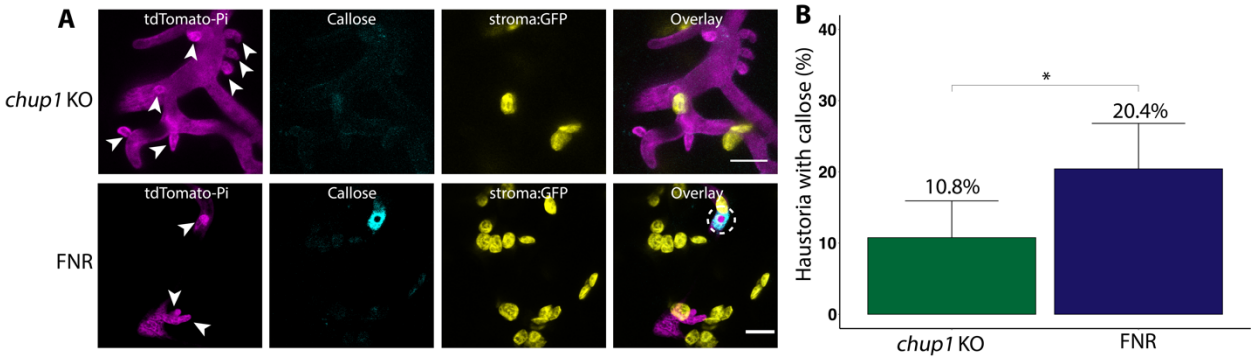

251

252 **Figure 3. CHUP1 contributes to callose deposition at haustorium penetration sites.** (A)
253 Confocal micrographs of *N. benthamiana* leaf epidermal cells of *chup1* KO plants and control
254 FNR plants. 4-week-old leaves were infected with tdTomato-expressing *P. infestans*, and stained
255 with aniline blue to visualize callose at 3 days post-infection. Images shown are maximum
256 projection of z-stack images. GFP channel depicts chloroplast stroma in *chup1* KO and FNR
257 plants. White arrows indicate haustoria. Scale bars represent 10 µm. (B) Bar graphs showing *chup1*
258 KO plants (10.8%, n = 130 haustoria) significantly reduce the frequency of callose deposition
259 around haustoria compared to control FNR plants (20.4%, N = 142 haustoria). Statistical
260 differences were analyzed by Fisher's exact test in R. Differences in measurements were
261 considered significant when $p<0.05$ (*).

262

263 **KACs contribute to plant immunity against *P. infestans* and callose deposition around the**
264 **haustoria**

265 The kinesin-like proteins KACs have genetically overlapping and independent functions with
266 CHUP1 in regulating chloroplast photorelocation[33,47]. Along with CHUP1, KACs are

267 indispensable for the polymerization and maintenance of cp-actin filaments[33,34,48]. Through cp-
268 actin filaments, these proteins are essential for both the proper movement of chloroplasts and their
269 association with the PM[33]. While they coordinately mediate cp-actin-mediated chloroplast
270 positioning, the underlying mechanism remains to be elucidated[38,47].

271 The *N. benthamiana* genome includes two KAC genes, *KAC1* and *KAC2*. Given that CHUP1 and
272 KACs have overlapping functions, we were intrigued to investigate if silencing KACs could confer
273 a susceptibility phenotype similar to that observed when CHUP1 is knocked out. To explore this,
274 we conducted infection assays upon downregulation of KAC expression. We employed a hairpin
275 silencing construct, RNAi:KAC, designed to specifically target *KAC1* and *KAC2* in *N.*
276 *benthamiana* (Figure S4). Similar to *CHUP1* silencing (Figures S1B and S1C), the silencing of
277 *KACs* using RNAi:KAC significantly increased *P. infestans* hyphal growth compared to the
278 control construct RNAi:GUS (Figures 4A and 4B). These results demonstrate that silencing *KACs*
279 confers plant susceptibility, highlighting their role in plant immunity against *P. infestans*.

280 We next investigated if KACs are also involved in focal immunity like CHUP1 (Figure 3). To
281 accomplish this, we performed aniline blue staining of infected plant cells upon VIGS of KACs
282 (Figure S4). We observed a reduction of approximately 44.9% (percentage change of frequency
283 from 28.5% to 12.8%) in the number of haustoria with callose deposits in VIGS:KAC plants
284 compared to VIGS:EV control plants (Figures 4C and 4D). These findings suggest that both
285 CHUP1 and KAC proteins play a role in focal immunity and are involved in proper callose
286 deposition at *P. infestans* haustoria.

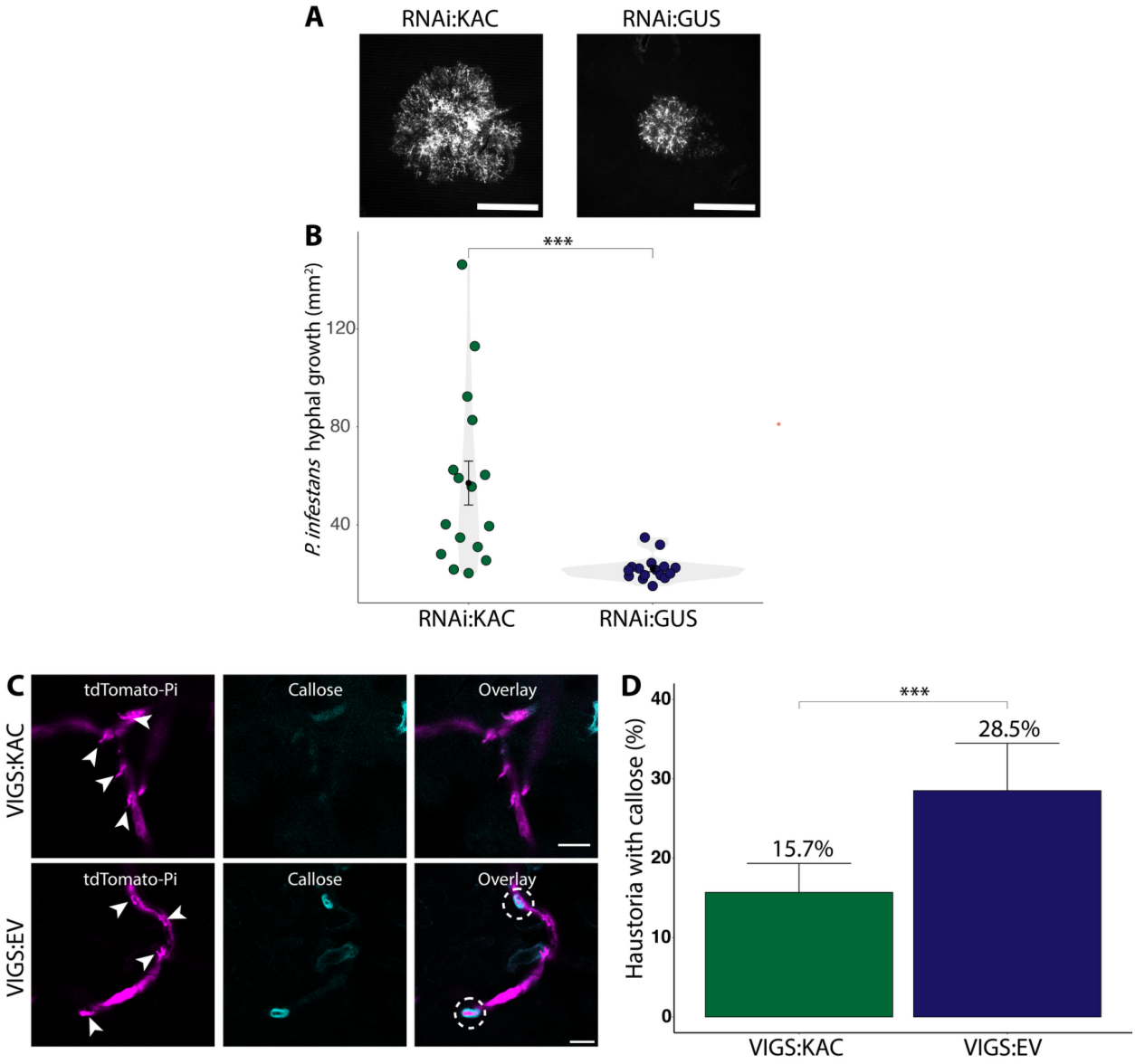

287

288 **Figure 4. KACs positively contribute to immunity against *Phytophthora infestans* and reduce**

289 **callose deposition surrounding *P. infestans* haustoria.** (A-B) Silencing *KAC* reduces hyphal

290 growth of *P. infestans*. (A) *N. benthamiana* leaves expressing RNAi:KAC, or RNAi:GUS control

291 were infected with tdTomato-expressing *P. infestans*, and pathogen growth was calculated by

292 measuring hyphal growth using fluorescence stereomicroscope at 5 days post-inoculation. Scale

293 bars represent 5 mm. (B) Violin plot illustrating that RNAi:KAC expression (57.1 mm^2, n = 48

294 infection spots) significantly increases *P. infestans* hyphal growth compared to RNAi:GUS control

295 (22.1 mm^2, n = 48 infection spots). Each dot represents the average of 3 infection spots on the
296 same leaf. Statistical differences were analyzed by Mann-Whitney U test in R. Measurements were
297 highly significant when $p < 0.001$ (***). (C-D) KAC proteins are involved in callose deposition at
298 haustorium penetration sites. (C) Confocal micrographs of VIGS:KAC and VIGS:EV control *N.*
299 *benthamiana* leaf epidermal cells. 4-week-old leaves were infected with tdTomato-expressing *P.*
300 *infestans*, and stained with aniline blue to visualize callose at 3 days post-infection. Images shown
301 are maximum projection of z-stack images. White arrows indicate haustoria. Scale bars represent
302 10 μm. (B) Bar graphs showing VIGS:KAC plants (15.69%, n = 376 haustoria) significantly
303 reduce the frequency of callose deposition around haustoria compared to control VIGS:EV plants
304 (28.51%, N = 221 haustoria). Statistical differences were analyzed by Fisher's exact test in R.
305 Differences in measurements were considered highly significant when $p<0.001$ (***).

306

307 **CHUP1 and KAC1 co-operate to tether chloroplasts to the pathogen interface**

308 Having identified that both CHUP1 and KAC proteins play similar positive roles in immunity and
309 are implicated in the focal immune responses against *P. infestans* haustoria, we aimed to explore
310 their potential interplay in membrane tethering of chloroplasts. To address this, we first expressed
311 C-terminally RFP-tagged KAC1 in *N. benthamiana* and investigated its localization pattern using
312 confocal microscopy. Unlike CHUP1, which localizes to the chloroplast outer envelope (Figures
313 2A, 2C and S2A), KAC1:RFP mainly localizes to the PM and cytosol (Figure S5A). However,
314 KAC1, similar to CHUP1 but not the control EV:RFP, accumulated at MCS between the
315 chloroplasts and the PM (Figures S5B and S5C). Remarkably, in *chup1* KO plants, KAC1 did not
316 show any accumulation at the chloroplast-PM contact sites (Figure S5D). This phenotype was
317 restored by the complementation of CHUP1:3xHA co-expression, but not the co-expression of the

318 empty vector control (3xHA:EV) (Figures S5D and S5E), demonstrating that KAC1 requires
319 CHUP1 to accumulate at MCS between chloroplasts and the PM. These results indicate that KAC1
320 might have a direct role in membrane anchoring of chloroplasts in cooperation with CHUP1. This
321 notion is consistent with the previous genetic studies implicating KAC1 and CHUP1 in chloroplast
322 anchoring to the PM in a co-operative manner, as neither mutant was able to show anchorage
323 independently[33,34]. Therefore, we next investigated the potential association between CHUP1 and
324 KAC1. Co-expression of KAC1:RFP and CHUP1:GFP in *N. benthamiana* revealed that both
325 proteins colocalize in punctate structures at MCS between chloroplasts and the PM (Figure S5F).
326 In contrast, the controls, Toc64:GFP and EV:RFP, did not form any punctate structures at these
327 MCS (Figures S5G and S5H), showing that not all chloroplast envelope proteins accumulate at the
328 PM contact sites and indicating that CHUP1 and KAC1 cooperate to anchor chloroplasts to
329 membranes.

330 Encouraged by these results, we next investigated KAC1-CHUP1 interplay in infected cells. In
331 haustoriated plant cells, we observed that CHUP1 colocalizes with KAC1 at punctate structures at
332 chloroplast-EHM MCS, whereas the empty vector control (EV:RFP) did not show such punctate
333 localization (Figures 5A, 5B, S6A and S6B). Furthermore, upon infecting *chup1* KO plants
334 expressing KAC1 with *P. infestans*, we found that KAC1 did not form puncta at chloroplast-EHM
335 MCS (Figures 5C and S6C). Complementing *chup1* KO plants with CHUP1:3xHA reinstated
336 KAC1 punctate formation at chloroplast-EHM MCS (Figures 5D and S6D). These findings
337 collectively suggest that KAC1 requires CHUP1 to anchor chloroplasts to the plant-pathogen
338 interface, presumably to execute their immune functions effectively. These results are consistent
339 with our previous findings, which demonstrated that chloroplasts are tightly tethered to the EHM,
340 as revealed by optical tweezer assays[7].

341 To further corroborate the interplay between CHUP1 and KAC1, we next investigated their *in*
342 *planta* interaction by performing co-immunoprecipitation (co-IP) assays. We co-expressed
343 KAC1:RFP alongside CHUP1:GFP, or controls Toc64:GFP and CHUP1^{Nterm}:GFP, the latter
344 containing the N-terminal region of CHUP1 required for localization to chloroplast outer
345 envelope[32]. Western blot analysis following GFP pulldowns revealed that KAC1:RFP interacts
346 with CHUP1:GFP but not with Toc64:GFP, CHUP1^{Nterm}:GFP, or EV:GFP (Figure 5E),
347 corroborating our confocal microscopy findings that the two proteins associate at chloroplast MCS
348 (Figures 5A, S5F and S6A).

349 CHUP1 is a modular protein that contains an actin-binding domain (ABD) necessary for the
350 formation of chloroplast-actin filaments (cp-actin), short actin filaments that accumulate at the
351 periphery of chloroplasts and the PM, which are implicated in chloroplast movement and PM
352 anchoring[31,35]. Therefore, we lastly investigated whether the actin-binding function of CHUP1 is
353 necessary for its complex formation with KAC1 and the formation of chloroplast-PM MCS. To
354 address this, we generated GFP fusions of CHUP1ΔABD, a CHUP1 construct lacking the actin-
355 binding domain. Confocal microscopy and co-IP assays revealed that the colocalization and
356 interaction of CHUP1 and KAC1 at MCS do not depend on the actin-binding ability of CHUP1
357 (Figures S7A and S7B). However, we noted a slight reduction in the amount of CHUP1 pulled
358 down with KAC1 when the actin-binding domain of CHUP1 was omitted (Figure S7B). We
359 conclude that while the ABD of CHUP1 is not essential for CHUP1-KAC1 interaction and their
360 assembly at chloroplast MCS, it could be important for coupling them more tightly to ensure secure
361 docking of chloroplasts at the PM and EHM. Collectively, our findings highlight that KAC1
362 interacts with CHUP1 and both proteins colocalize at crucial membrane contact sites, facilitating
363 the anchoring of chloroplasts to the PM and the plant-pathogen interface.

364

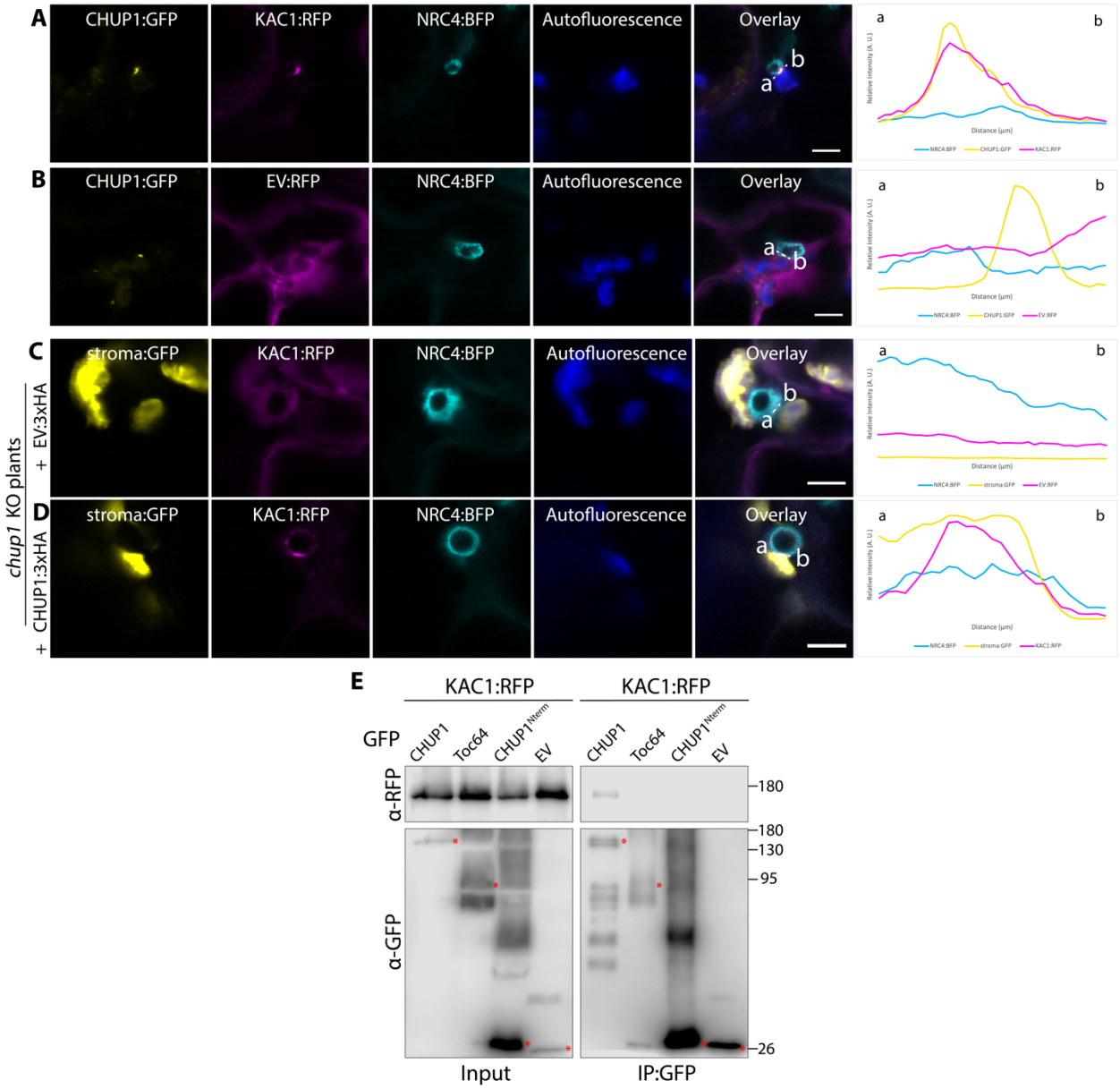

365

366 **Figure 5. KAC1 interacts with CHUP1 and they colocalize at chloroplast-EHM MCS.** (A-B)
367 CHUP1 colocalizes with KAC1 at punctate structures at chloroplast-EHM MCS. Confocal
368 micrographs of *N. benthamiana* leaf epidermal cells transiently expressing CHUP1:GFP and
369 NRC4:BFP, with (A) KAC1:RFP, or (B) EV:RFP. NRC4:BFP acts as an EHM marker. The leaves
370 were infected with WT *P. infestans* spores at 6 hpi, and imaged at 3 dpi. (C-D) CHUP1 is required

371 for KAC1 to form punctate structures at chloroplast-EHM MCS. Confocal micrographs of *chup1*
372 KO *N. benthamiana* leaf epidermal cells transiently expressing KAC1:RFP and NRC4:BFP with
373 (C) EV:3xHA, or (D) CHUP1:3xHA. NRC4:BFP acts as an EHM marker. The leaves were
374 infected with WT *P. infestans* spores at 6 hpi, and imaged at 3 dpi. All presented confocal images
375 are single plane images. Autofluorescence channel depicts chloroplasts. GFP channel depicts
376 chloroplast stroma in *chup1* KO plants. Transects in overlay panels correspond to line intensity
377 plots depicting the relative fluorescence across the marked distance. Scale bars represent 5 µm.
378 (E) KAC1 interacts with full length CHUP1, but not with Toc64, CHUP1^{Nterm}, or EV:GFP.
379 KAC1:RFP was transiently co-expressed with either CHUP1:GFP, Toc64:GFP, CHUP1^{Nterm}:GFP,
380 or EV:GFP. IPs were obtained with anti-GFP antibody. Total protein extracts were immunoblotted.
381 Red asterisks indicate band sizes. Numbers on the right indicate kDa values.

382

383 **Discussion**

384

385 Here, we uncovered MCS between chloroplasts and the EHM in *P. infestans*-infected plant cells.
386 We reveal that these MCS are required for proper immune responses and consist of a membrane
387 anchoring complex comprising the chloroplast outer envelope protein CHUP1 and the PM-
388 associated protein KAC1. Our genetic and cell biology analyses revealed that KAC1 marks these
389 MCS only in the presence of CHUP1. Additionally, our biochemical assays show that CHUP1 and
390 KAC1 interact. We propose a model in which CHUP1 and KAC1 synergistically contribute to
391 plant focal immunity by facilitating MCS at the pathogen penetration sites during infection (Figure
392 6).

393 The role of CHUP1-KAC1 MCS in pathogen resistance is underscored by our findings that
394 depletion of CHUP1 or KAC1 leads to enhanced susceptibility to the adapted pathogen *P. infestans*
395 (Figures 1 and 4). This susceptibility is accompanied by a reduction in focal immune responses,
396 as evidenced by decreased callose accumulation around the haustorium, without affecting other
397 core immune processes (Figures 3, 4 and S3). These results align with findings from other studies
398 showing that *CHUP1* knockouts in Arabidopsis similarly result in decreased penetration resistance
399 to non-adapted pathogens[36]. Additionally, previous studies have implicated chloroplast outer
400 envelope proteins AtNHRA/B in the proper accumulation of callose[49], further supporting our
401 observations that chloroplasts contribute to callose accumulation around the haustorium.

402 Prior research has also revealed that mitochondria accumulates at pathogen penetration sites and
403 contribute to pathogen penetration resistance, although it remains unknown whether mitochondria
404 can associate with the EHM[8]. Our previous work using optical tweezers showed that chloroplasts
405 can be tightly tethered to the EHM[7], but the mechanisms and reasons for this remained unknown.
406 While the precise mechanism by which CHUP1-KAC1 mediates callose deposition around the
407 haustorium remains unknown, their role in tethering chloroplasts to the EHM suggests a significant
408 involvement of chloroplasts in resistance to pathogen penetration. These tethers could ensure
409 secure membrane contacts, facilitating potential short distance material transport through
410 chloroplast-EHM conduits. Indeed, one of the key features of MCS is the direct transfer of lipids,
411 proteins, signaling molecules, ions and metabolites. It is conceivable that CHUP1-KAC1-labeled
412 MCS facilitate the transport of biochemical precursors necessary for callose synthesis or the
413 transfer of ROS that cross-link and fortify callose deposits[50-52]. These MCS may act as critical
414 hubs for the exchange of materials and signals essential for reinforcing the cell wall at pathogen
415 entry points.

416 Our current understanding of the mechanisms of chloroplast movement and membrane anchoring
417 originates from studies focusing on chloroplast photorelocation, a process for maximizing
418 photosynthesis and minimizing photodamage based on exposure to light intensities. While dozens
419 of proteins are implicated in chloroplast movement, the detailed molecular interactions and
420 mechanisms remain largely elusive. Previous genetic studies have identified CHUP1 and KAC1
421 as key players in chloroplast photorelocation[33,47,53]. Our findings align with this, showing that
422 CHUP1 accumulates at foci where chloroplasts contact the PM (Figure 2A). Additionally, we
423 observed that CHUP1 also localizes at EHM contact sites (Figure 2C), and that KAC1 accumulates
424 at these sites in a CHUP1-dependent manner (Figures 5C, 5D, S5D and S5E). Our biochemical
425 assays further support the physical interaction between CHUP1 and KAC1 (Figures 5E and S7B).
426 These results suggest that the machinery involved in chloroplast photorelocation is co-opted for
427 innate immune responses. Furthermore, blue light receptors, which regulate chloroplast
428 photorelocation, are also implicated in plant immunity[54,55], underscoring the multifaceted role of
429 these components in both light response and pathogen defense mechanisms.

430 The exact biochemical and molecular mechanisms through which CHUP1 and KAC1 facilitate
431 MCS tethering chloroplasts to the pathogen interface and contribute to pathogen resistance are yet
432 to be fully elucidated. Future studies are required to determine how these MCS formed by CHUP1
433 and KAC1 enhance immune responses. Investigating the dynamics of these contact sites and their
434 precise molecular and biochemical functions will be crucial in understanding how they contribute
435 to the targeted deposition of defense components at the pathogen interface. Understanding the
436 intricacies of MCS at the pathogen interface will provide deeper insights into plant defense
437 mechanisms and could inform the development of new strategies to enhance crop disease
438 resistance.

439

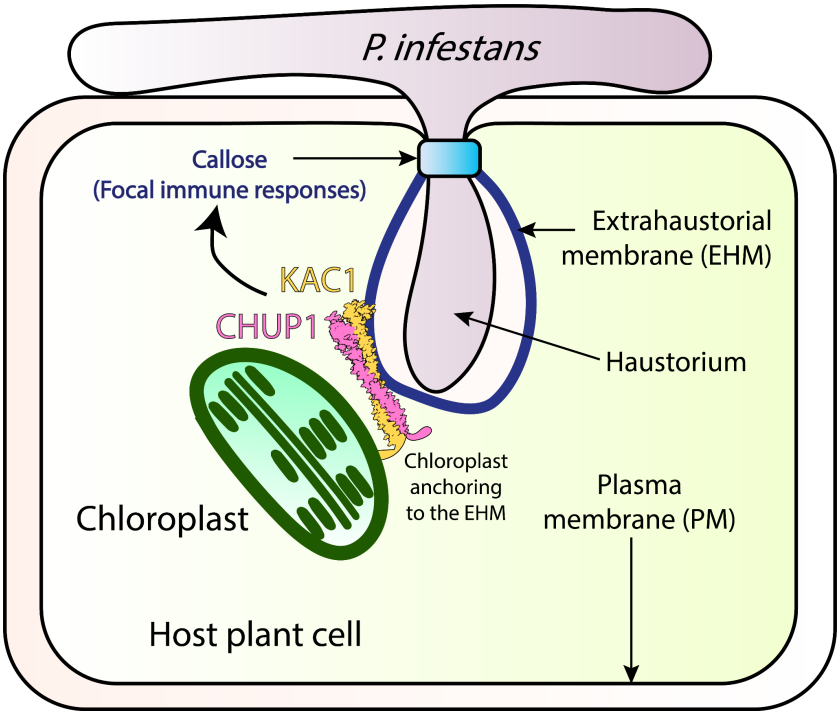

440

441 **Figure 6. Summary model of CHUP1 and KAC1 coordinating to anchor chloroplasts to the**
442 **extrahaustorial membrane and contribute to plant focal immunity.** *P. infestans* penetrates the
443 host plant cell by forming a specialized structure called the haustorium, which is surrounded by a
444 host-derived extrahaustorial membrane (EHM) that acts as the plant-pathogen interface. The
445 chloroplast movement-associated proteins CHUP1 and KAC1 interact to form chloroplast-EHM
446 membrane contact sites (MCS), thereby anchoring chloroplasts to the EHM. This interaction
447 contributes to plant focal immunity, such as callose deposition and potentially other immune
448 responses at the plant-pathogen interface.

449

450

451

452 **Materials and Methods**

453

454 **Plant growth details**

455 *Nicotiana benthamiana* plants (wild-type and transgenics) were cultivated under controlled
456 conditions in a growth chamber maintained at a temperature of 24°C. They were grown in a
457 substrate mixture comprising organic soil (3:1 ratio of Levington's F2 with sand and Sinclair's 2-
458 5 mm vermiculite). The plants were exposed to high-intensity light and subjected to a long-day
459 photoperiod (16 hours of light followed by 8 hours of darkness). Experiments were conducted
460 using plants aged 4 to 5 weeks. Among the transgenic plants utilized were CP plants[7], expressing
461 GFP in the chloroplast stroma, and FNR plants[56], expressing FNR:eGFP in the chloroplast. FNR
462 plants served as the parental lines for *chup1* KO plants and were employed as controls in *chup1*
463 KO experiments.

464

465 **Pathogen growth details and infection assay**

466 WT and tdTomato-expressing *Pytophthora infestans* 88069 isolates were cultured on rye sucrose
467 agar (RSA) medium in darkness at 18°C for 10 to 15 days before harvesting zoospores. Zoospores
468 were collected by adding cold water at 4°C to the medium and then incubating it in darkness at
469 4°C for 90 minutes. For the infection assay, 10 µl droplets of zoospore solution containing 50,000
470 spores/ml were applied to the underside of leaves. The leaves were subsequently maintained in a
471 humid environment. Confocal microscopy was conducted 3 days post-infection, and fluorescent
472 images were captured at 5 days post-infection. Hyphal growth was quantified and analyzed using
473 ImageJ.

474

475 **Generation of *N. benthamiana* CHUP1 CRISPR knockout plants**

476 To generate *chup1* KO and *chup1* KO#2 plants, the following primer pairs were used to create
477 guide RNA sequences targeting both *NbChup1* alleles: attGCAAGATCAAGGAGTTGCAG &
478 aaacCTGCAACTCCTTGATCTTG; attgTGGACTTCAAGAAAAGGAAG &
479 aaacCTTCCTTTTCTTGAAGTCCA; and attgTCTGTATCATACTTGTCACT &
480 aaacAGTGACAAGTATGATACAGA. The genome editing vector used was pDGE463[57]. This
481 vector contains: plant kanamycin resistance for positive selection of transgenic plants, the Bs3
482 gene from pepper for negative selection, 2xtagRFP expressed by a seed coat-specific promoter for
483 negative selection, a p35S-driven intronized Cas9 with 2xNLS for targeted gene editing, and
484 bacterial spectinomycin resistance for selection in bacteria. The guide RNAs were inserted into
485 pDGE463 to create the new vector, pDGE472. The primers used for genotyping *chup1* KO plants
486 were CHUP1KO_genotype_F and CHUP1KO_genotype_R, while the primers used for
487 genotyping *chup1* KO#2 plants were CHUP1KO2_genotype_F and CHUP1KO2_genotype_R.
488 The parental line transformed was NbFNR:eGFP_7-25 (FNR) for *chup1* KO plants[58], and the
489 parental line transformed was wild-type (WT) for *chup1* KO#2 plants.

490

491 **Molecular cloning**

492 The molecular cloning of KAC1, CHUP1, CHUP1^{Nterm}, CHUP1ΔABD, MEK2^{DD}, and NLS was
493 conducted using Gibson Assembly, following the methods described in previous works[3,59].
494 Specifically, the vector backbone was a pK7WGF2 derivative domesticated for Gibson Assembly,
495 containing a C-terminal fluorescent GFP, RFP, BFP, or 3xHA tag. The desired sequences for
496 cloning were either manufactured as a synthetic fragment or amplified using designed primers as
497 detailed in Table S1 and S2. CHUP1ΔABD was created using two fragments that were amplified

498 with two sets of primers, excluding the actin-binding domain flanked by the fragments. The
499 fragments were then inserted into the vector using Gibson Assembly and transformed into DH5α
500 chemically competent *E. coli* through heat shock. These plasmids were subsequently amplified
501 and extracted using the PureYield™ Plasmid Miniprep System (Promega), and electroporated into
502 *Agrobacterium tumefaciens* GV3101 electrocompetent cells. Sequencing was done by Eurofins.
503 LB agar containing gentamicin and spectinomycin was used to grow bacteria carrying the
504 pK7WGF2 plasmid. The NLS:BFP construct was created by joining a cut pK7WGF2-derived C-
505 terminal BFP vector with a single-stranded DNA oligo bridge using Gibson assembly. The single-
506 stranded DNA oligo bridge had overhangs complementary to the cut vector ends and included the
507 coding sequence for the SV40 nuclear localization sequence (PKKKRKVEDP). For virus-induced
508 gene silencing (VIGS), TRV2:CHUP1 was constructed by amplifying a region of the CHUP1
509 sequence using the primer pair CHUP1_sil_F and CHUP1_sil_R. The amplified fragment was then
510 cloned into a Gateway-compatible pTRV2 vector using Gateway cloning technology (Invitrogen).
511 TRV2:KAC for VIGS was constructed by amplifying a region of the KAC1 sequence using the
512 primer pair KAC1_sil_F and KAC1_sil_R. The amplified fragment was then cloned into a Golden
513 Gate-compatible TRV2-GG vector using Golden Gate cloning[60]. LB agar containing gentamicin
514 and kanamycin was used to grow bacteria carrying pTRV2 and TRV2-GG plasmids. For the RNA
515 interference (RNAi) silencing construct RNAi:KAC, an intron-containing hairpin RNA vector for
516 RNA interference in plants (pRNAi-GG) was employed, based on the Golden Gate cloning method
517 described in previous studies[3,61]. RNAi:KAC targeted the region between 3512 and 3709 bp of
518 *NbKAC1/2*. The target fragment was amplified using KAC1_sil_F and KAC1_sil_R and then
519 inserted into the pRNAi-GG vector in both sense and antisense orientations, utilizing the
520 overhangs left by BsaI cleavage. This resulted in the expression of a construct that folds back onto

521 itself, forming the silencing hairpin structure. The subsequent steps of *E. coli* transformation,
522 Miniprep, sequencing, and Agrobacterium transformation were the same as those used for the
523 overexpression constructs. LB agar containing gentamicin, kanamycin, and chloramphenicol was
524 used to grow bacteria carrying the pRNAi-GG plasmid. All primers and synthetic fragments used
525 in this study are detailed in Table S1. All constructs used in this study are detailed in Table S2.
526

527 **Confocal laser scanning microscopy**

528 The confocal microscopy analyses were conducted three days following agroinfiltration. To
529 visualize the leaf tissue, the leaves were excised using a size 4 cork borer, mounted live on glass
530 slides, and submerged in wells of dH_2O using Carolina observation gel (Carolina Biological).
531 Imaging of the abaxial side of the leaf tissue was performed using either a Leica TCS SP8 inverted
532 confocal microscope equipped with a 40x water immersion objective lens or a Leica STELLARIS
533 5 inverted confocal microscope equipped with a 63x water immersion objective lens. Laser
534 excitations for GFP, RFP/tdTomato, and BFP tags were set at Argon 488 nm (15%), DPSS 561
535 nm, and Diode 405 nm, respectively. Emission ranges for GFP, RFP/tdTomato, and BFP tags were
536 495 - 550 nm, 570 - 620 nm, and 402 - 457 nm, respectively. To prevent spectral overlap from
537 different fluorescent tags when imaging samples with multiple tags, sequential scanning between
538 lines was employed. Confocal images were analyzed using ImageJ.
539

540 **Confocal Image analysis**

541 The number of chloroplasts was automatically counted using ImageJ. Maximum intensity z-
542 projections of z-stack images were created, and the channels were split. The autofluorescence
543 channel was then automatically thresholded using the "Li" method, followed by the application of

544 a watershed. Objects were counted using the "Analyze Particles" command with a size filter of 5-
545 35.
546
547 For quantifying chloroplast-haustoria association, haustoria were first identified in a given z-stack
548 using only the RFP and brightfield channels to ensure that their identification was not influenced
549 by the position of chloroplasts. The number of haustoria associated with a chloroplast, including
550 those connected via a stromule, was then counted. The percentage of haustoria associated with
551 chloroplasts was calculated based on the total number of identified haustoria. To avoid skewing
552 the data with images containing a single haustorium, which could result in extreme percentages
553 (0% or 100%), the overall percentage for the entire data set was used instead of calculating
554 percentages on an image-by-image basis.
555
556 Quantifying perinuclear chloroplast clustering was challenging due to the close packing of
557 chloroplasts around the nucleus, making it difficult to resolve individual chloroplasts. To measure
558 perinuclear clustering, the total volume of thresholded chlorophyll autofluorescence around the
559 nuclei was quantified. First, nuclei were automatically identified from maximum intensity z-
560 projections of z-stack images, with channels split. The NLS:BFP channel was automatically
561 thresholded using the "Li" method, followed by the application of a watershed. Nuclei were then
562 counted using the "Analyze Particles" command with a size filter of 100-500. The positions of the
563 identified nuclei were saved as regions of interest (ROIs). For each ROI, the original image was
564 duplicated and cropped to a 70x70 pixel region around the nucleus, which was then saved
565 separately for further analysis. The quality of these cropped images was manually assessed. If
566 necessary, the following adjustments were made: a) Slices of the z-stack containing the mesophyll

567 layer were removed. b) Crops were resized to exclude chloroplasts from adjacent cells or those not
568 in immediate contact with the nucleus. The chloroplast autofluorescence channel was then isolated
569 and automatically thresholded using the "Li" method. For each slice of the z-stack, pixels with a
570 value of 255 were counted, and the voxel size was determined for each image. This data was
571 compiled into a custom table containing pixel count, voxel size, and image name for all identified
572 nuclei. Using this table, the cubic microns of thresholded chloroplast autofluorescence were
573 calculated for each identified nucleus, providing a metric for perinuclear chloroplast clustering.
574

575 **Fluorescence microscopy for *N. benthamiana***

576 Fluorescence microscopy was employed to observe the hyphal growth of *P. infestans* expressing
577 tdTomato. The imaging setup included a Leica MZ 16 F microscope paired with the Leica DFC300
578 FX Digital Color Camera, specifically designed for fluorescence imaging. Infected leaf samples
579 were placed on a petri dish within the imaging zone of the microscope. The imaging filter utilized
580 was DsRed, with an excitation range ranging from 510 to 560 nm.
581

582 **Agrobacterium-mediated transient gene expression in *N. benthamiana***

583 Agrobacterium-mediated transient gene expression was carried out via agroinfiltration, following
584 a well-established protocol[1]. *Agrobacterium tumefaciens* containing the desired plasmid was
585 rinsed with water and then suspended in agroinfiltration buffer (10 mM MES, 10 mM $MgCl_2$, pH
586 5.7). The optical density (OD_{600}) of the bacterial suspension was measured using the
587 BioPhotometer spectrophotometer (Eppendorf). Subsequently, the suspension was adjusted to the
588 required OD_{600} according to the specific construct and experimental conditions. The adjusted

589 bacterial suspension was then infiltrated into *N. benthamiana* leaf tissue aged 3 to 4 weeks using
590 a needleless 1ml Plastipak syringe.
591
592 **RNA isolation, cDNA synthesis, and RT-PCR**
593 To perform RNA extraction, 56 - 70 mg of leaf tissue was promptly frozen in liquid nitrogen. The
594 RNA extraction process employed the Absolutely Total RNA Purification Kits (Agilent
595 Technologies). Subsequently, RNA concentration was quantified using NanoDrop Lite
596 Spectrophotometer (Thermo Scientific). 2 mg of the extracted RNA underwent treatment with
597 RQ1 RNase-Free DNAse (Promega) before being used for cDNA synthesis with SuperScript IV
598 Reverse Transcriptase (Invitrogen). The resulting cDNA was then amplified using Phusion High-
599 Fidelity DNA Polymerase (New England Biolabs) or DreamTaq DNA polymerase (Thermo
600 Scientific). *GAPDH* transcription level was utilized as the transcriptional control. The RT-PCR for
601 *GAPDH* was performed using the primers GAPDH_RTPCR_F and GAPDH_RTPCR_R. The RT-
602 PCR confirming VIGS:CHUP1 was performed using the primers NbCHUP1a_RTPCR_F and
603 NbCHUP1a_RTPCR_R for *NbCHUP1a* and NbCHUP1b_RTPCR_F and
604 NbCHUP1b_RTPCR_R for *NbCHUP1b*. The RT-PCR confirming RNAi:KAC and VIGS:KAC
605 was performed using the primers KAC1_RTPCR_F and KAC1_RTPCR_R for *NbKAC1* and
606 KAC2_RTPCR_F and KAC2_RTPCR_R for *NbKAC2*. All primers used in this study are detailed
607 in Table S1.
608
609 **Chlorophyll extraction**
610 Three leaf discs, obtained with a size 4 cork borer, were collected from three distinct leaves of
611 each plant. Each leaf disc was then ground in 10 mL of methanol for 1 minute and centrifuged at

612 2000 rpm for 5 minutes. Absorbance readings at 666 and 653 nm were recorded, and the total
613 chlorophyll concentration was determined following a well-established method detailed by
614 Wellburn et al[62].
615
616 **Co-immunoprecipitation and immunoblot analyses**
617 Proteins were transiently expressed in *N. benthamiana* leaves through agroinfiltration, and the
618 harvest took place 3 days after agroinfiltration. Co-immunoprecipitation experiments utilized 2 g
619 of leaf tissues. The procedures for protein extraction, purification, and immunoblot analysis
620 followed the previously described protocols[1]. The primary antibodies used included monoclonal
621 anti-RFP produced in mouse (Chromotek), monoclonal anti-GFP produced in rat (Chromotek),
622 polyclonal anti-phospho-MAPK produced in rabbit (Cell Signaling Technology), and monoclonal
623 HRP-conjugated anti-beta actin produced in mouse (Proteintech). As for secondary antibodies,
624 anti-rabbit antibody (Sigma-Aldrich), anti-rat antibody (Sigma-Aldrich), and anti-mouse antibody
625 (Sigma-Aldrich) for HRP detection were employed. Comprehensive information regarding the
626 antibodies used is detailed below.
627
628 List of antibodies used in this research:

Primary/Secondary	**Detail**	**Company**	**Product Code**
Primary	Anti-GFP (Rat monoclonal)	Chromotek	3H9
Primary	Anti-RFP (Mouse monoclonal)	Chromotek	6G6
Primary	Anti-phospho-MAPK (Rabbit polyclonal)	Cell Signaling Technology	9101

Secondary	Anti-rabbit (HRP)	Sigma-Aldrich	A9169
Secondary	Anti-rat (HRP)	Sigma-Aldrich	A9037
Secondary	Anti-mouse (HRP)	Sigma-Aldrich	SAB3700986
Primary/Secondary	HRP-conjugated anti-beta actin (Mouse monoclonal)	Proteintech	HRP-60008

629

630 **Cell death assay**

631 Cell death inducers were introduced into the underside of *N. benthamiana* leaves via
632 agroinfiltration. Afterward, at 3 dpi, the leaves were detached and examined under both natural
633 light conditions. The degree of cell death was assessed using an established seven-tiered cell death
634 scale[63].

635

636 ***Phytophthora infestans* extract (Pi extract) preparation and injection**

637 Mycelia harvested from *P. infestans* RSA plates were gathered and suspended in 5 ml of water per
638 petri dish. The suspension underwent vortexing for 1 minute and was then subjected to heating at
639 95°C for 20 minutes. Following this, the mixture was filtered through filter paper with a pore size
640 ranging from 5 to 13 µm. The resulting filtrate underwent an additional filtration step using a
641 syringe filter with a pore size of 0.45 µm. This resulting solution was then administered to plants
642 to function as a PAMP cocktail, and is stored at -20ºC.

643

644

645

646 **Virus-induced gene silencing (VIGS)**

647 Agrobacterium was prepared as described above, carrying TRV1 and the respective TRV2
648 construct, and mixed to achieve final OD_{600} values of 0.4 or 0.2, respectively, in agroinfiltration
649 buffer supplemented with 100 μM acetosyringone (Sigma-Aldrich). The mixture was then kept in
650 the dark for 2 hours prior to infiltration to enhance virulence. Fourteen-day-old *N. benthamiana*
651 seedlings were infiltrated in both cotyledons and any emerged true leaves. For CHUP1-silencing,
652 *N. benthamiana* plants were infiltrated with TRV1 and TRV2:CHUP1, while for KAC1-silencing,
653 TRV1 and TRV2:KAC were used. The empty vector control was achieved by infiltrating TRV1
654 and TRV2:EV. Plants were allowed to grow under standard conditions until experiments could be
655 conducted three weeks later.

656

657 **Image processing and data analysis**

658 The confocal microscopy images were processed using Leica LAS X software and ImageJ. ImageJ
659 was employed for analyzing and quantifying the infection assay experiments. Data were presented
660 using violin plots, box plots and bar graphs created with R. Statistical differences were evaluated
661 using appropriate tests that consider normality and variance. Significance levels were denoted as
662 follows: * ($p < 0.05$), ** ($p < 0.01$), and *** ($p < 0.001$). Detailed information regarding the
663 statistical tests utilized can be found in the figure captions, and extensive statistical calculations
664 are available in Table S3.

665

666

667

668

669 **Accession numbers**

670 CHUP1a (Sol Genomics Network: Niben101Scf00570g03008/9.1; NbenBase:
671 Nbe.v1.1.chr08g25910); CHUP1b (Sol Genomics Network: Niben101Scf01338g03019.1); KAC1
672 (NbenBase: Nbe.v1.1.chr13g42800); KAC2 (NbenBase: Nbe.v1.1.chr05g36640).

673

674 **Acknowledgments**

675 We gratefully acknowledge the technical expertise and access to microscopy equipment provided
676 by the Imperial College FILM facility.

677

678 **Funding**

679 BBSRC grants BB/X511055/1 and BB/X016382/1 (E.L.H.Y.); BBSRC grant BB/M011224/1
680 (C.D.); BBSRC grant BB/T006102/1 (Y.T., T.O.B.); Research in M.S. lab (J.L.E., J.P., M.S.) is
681 funded by the Deutsche Forschungsgemeinschaft (DFG, German Research Foundation) –
682 400681449/GRK2498 as well as Martin-Luther-University core funding.

683

684 **Author contributions**

685 Conceptualization: E.L.H.Y., Z.S., M.S., T.O.B.

686 Methodology: E.L.H.Y., Z.S., M.S., T.O.B.

687 Validation: E.L.H.Y., Z.S., V.A., C.V., Y.Z., F.R., A.I.B.

688 Formal Analysis: E.L.H.Y., Z.S., V.A., C.V., Y.Z., A.I.B.

689 Investigation: E.L.H.Y., Z.S., V.A., C.V., Y.Z., F.R., A.I.B.

690 Resources: E.L.H.Y., Z.S., V.A., Y.T., J.L.E., J.P., J.S., C.D., C.M.

691 Data Curation: E.L.H.Y., T.O.B.

Visualization: E.L.H.Y., Z.S.

Writing – Original Draft: E.L.H.Y., Z.S., T.O.B.

Writing – Review & Editing: E.L.H.Y., Y.T., T.O.B.

Supervision: E.L.H.Y., Z.S., M.S., T.O.B.

Funding Acquisition: M.S., T.O.B.

Competing interest statement

T.B. and C.D. receive funding from industry on NLR biology. T.B. and C.D. are co-founders of Resurrect Bio Ltd. The remaining authors have no conflicts of interest to declare.

Declaration of generative AI and AI-assisted technologies in the writing process

During the preparation of this work, the authors used ChatGPT to check grammar and phrasing. After using ChatGPT, the authors reviewed and edited the content as needed and take full responsibility for the content of the publication.

Data and materials availability

All relevant study data are included in the article, and in the Supplementary Materials files.

Supplementary Materials in this combined PDF include the following:

Supplementary Figures S1-S7

Supplementary Tables S1-S2

Other Supplementary Materials for this manuscript include the following:

Table S3. Summary of Statistics

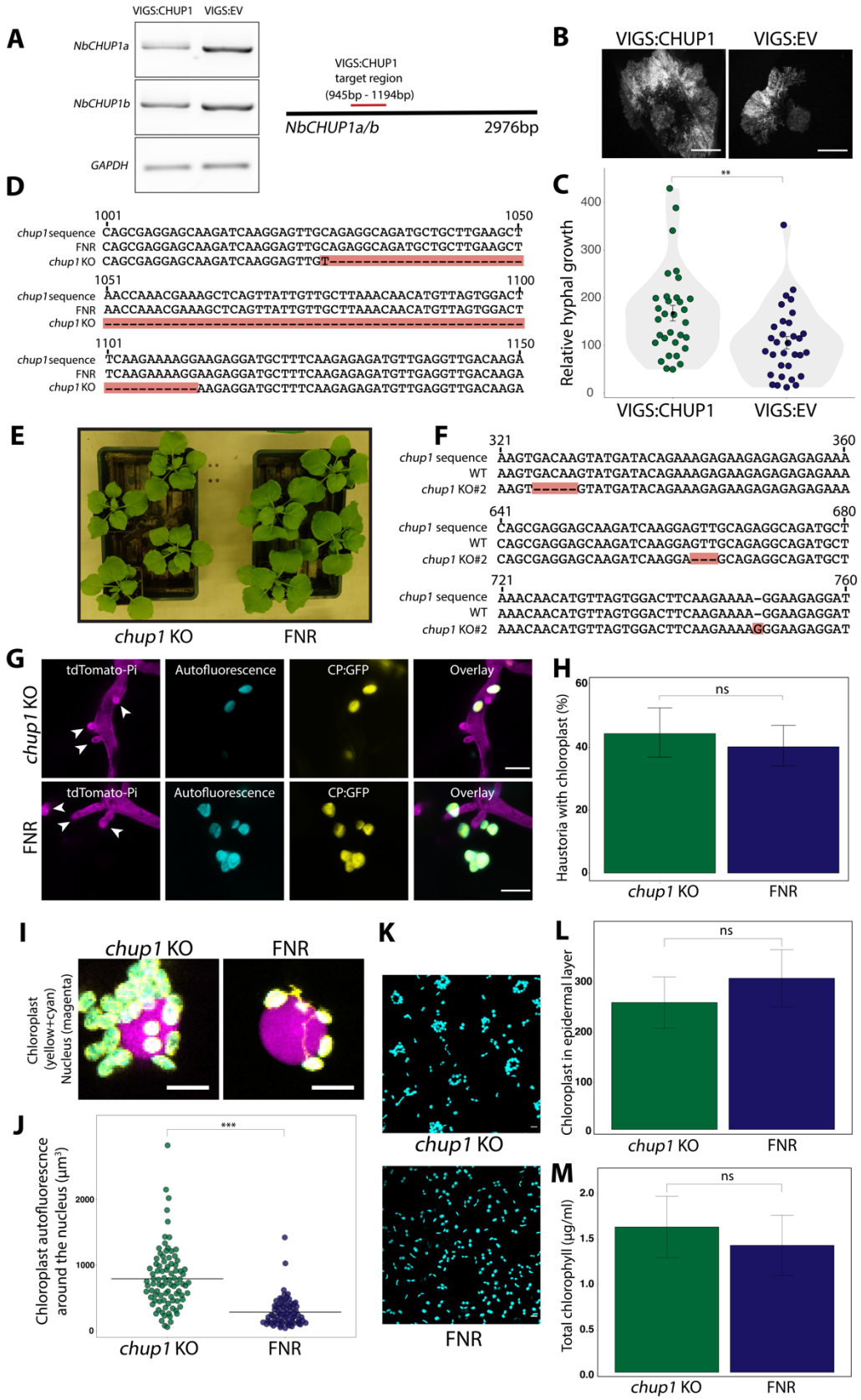
A
VIGS:CHUP1
VIGS:EV
NbCHUP1a
NbCHUP1b
GAPDH
VIGS:CHUP1
target region
(945bp - 1194bp)
NbCHUP1a/b
2976bp
B
VIGS:CHUP1
VIGS:EV
C
Relative hyphal growth
VIGS:CHUP1
VIGS:EV
D
1001
1050
chup1 sequence CAGCGAGGAGCAAGATCAAGGAGTTGCAGAGGCAGATGCTGCTTGAAGCT
FNR CAGCGAGGAGCAAGATCAAGGAGTTGCAGAGGCAGATGCTGCTTGAAGCT
chup1 KO CAGCGAGGAGCAAGATCAAGGAGTTGT
1051
1100
chup1 sequence AACCAAACGAAAGCTCAGTTATTGTTGCTTAAACAACATGTTAGTGGACT
FNR AACCAAACGAAAGCTCAGTTATTGTTGCTTAAACAACATGTTAGTGGACT
chup1 KO
1101
1150
chup1 sequence TCAAGAAAAGGAAGAGGATGCTTTCAAGAGAGATGTTGAGGTTGACAAGA
FNR TCAAGAAAAGGAAGAGGATGCTTTCAAGAGAGATGTTGAGGTTGACAAGA
chup1 KO AAGAGGATGCTTTCAAGAGAGATGTTGAGGTTGACAAGA
E
chup1 KO
FNR
F
321
360
chup1 sequence AAGTGACAAGTATGATACAGAAAGAGAAGAGAGAGAGAAA
WT AAGTGACAAGTATGATACAGAAAGAGAAGAGAGAGAGAAA
chup1 KO#2 AAGTGTATGATACAGAAAGAGAAGAGAGAGAGAAA
641
680
chup1 sequence CAGCGAGGAGCAAGATCAAGGAGTTGCAGAGGCAGATGCT
WT CAGCGAGGAGCAAGATCAAGGAGTTGCAGAGGCAGATGCT
chup1 KO#2 CAGCGAGGAGCAAGATCAAGGAGCAGAGGCAGATGCT
721
760
chup1 sequence AAACAACATGTTAGTGGACTTCAAGAAAA-GGAAGAGGAT
WT AAACAACATGTTAGTGGACTTCAAGAAAA-GGAAGAGGAT
chup1 KO#2 AAACAACATGTTAGTGGACTTCAAGAAAAGGGAAGAGGAT
G
chup1 KO
FNR
tdTomato-Pi
Autofluorescence
CP:GFP
Overlay
H
Haustoria with chloroplast (%)
ns
chup1 KO
FNR
I
chup1 KO
FNR
Chloroplast (yellow+cyan)
Nucleus (magenta)
J
Chloroplast autofluorescnce around the nucleus (μm³)
***
chup1 KO
FNR
K
chup1 KO
FNR
L
Chloroplast in epidermal layer
ns
chup1 KO
FNR
M
Total chlorophyll (μg/ml)
ns
chup1 KO
FNR

725

726 **Figure S1. CHUP1 positively contributes to plant immunity and the increased disease**
727 **susceptibility observed in *chup1* KO plants is not attributed to impaired chloroplast**
728 **positioning or abnormal chloroplast numbers.** (A) Validation of *CHUP1* silencing of
729 VIGS:CHUP1 plants. Constructs carrying TRV1 with TRV2-GG targeting *NbCHUP1a and*
730 *NbCHUP1b* or the control TRV2:EV were infiltrated to *N. benthamiana* leaves. The expression
731 levels of the targeted genes were assessed via RT-PCR at 3 weeks post VIGS. The RT-PCR
732 employs primers NbCHUP1a_RTPCR_F and NbCHUP1a_RTPCR_R for *NbCHUP1a*, and
733 NbCHUP1b_RTPCR_F and NbCHUP1b_RTPCR_R for *NbCHUP1b*. RT-PCR results confirmed
734 gene silencing of *NbCHUP1a* and *NbCHUP1b* in the VIGS:CHUP1 plants. Glyceraldehyde 3-
735 phosphate dehydrogenase (GAPDH) served as the internal control, using primers
736 GAPDH_RTPCR_F and GAPDH_RTPCR_R for assessment. The cDNA was synthesized using
737 total RNA. (B) WT *N. benthamiana* leaves were infected with tdTomato-expressing *P. infestans*
738 3 weeks post VIGS, and pathogen growth was calculated by measuring hyphal growth using
739 fluorescence stereomicroscope at 5 days post-inoculation. Scale bars represent 5 mm. (C) Violin
740 plot illustrating that plants treated with VIGS:CHUP1 construct (167.7, n = 192 infection spots)
741 show a significant increase in *P. infestans* hyphal growth compared to plants treated with control
742 VIGS:EV construct (105.6, n = 192 infection spots). Each dot represents the average of 6 infection
743 spots on the same leaf. Statistical differences were analyzed by Mann-Whitney U test in R.
744 Measurements were significant when $p<0.01$. (**). (D) Generation of *N. benthamiana chup1*
745 CRISPR knockout mutant, designated as *chup1* KO plants, in an FNR:eGFP background. *chup1*
746 KO plants contain a 84 nt deletion that introduces premature stop codons in the *chup1* gene. (E)
747 Daylight photographs of representative four-week-old *chup1* KO and FNR plants used for
748 experiments. (F) Generation of *N. benthamiana chup1* CRISPR knockout mutant, designated as

749 *chup1* KO#2 plants, in a WT background. *chup1* KO#2 plants contain three editing sites in the
750 *chup1* gene. First site contains a 5 nt deletion and causes a frameshift with stop codons
751 downstream. Second site contains a 3 nt deletion. Third site contains a 1 nt insertion. These
752 mutations do not reconstitute the reading frame. (G-H) Chloroplast positioning at haustoria is
753 unaffected by the loss of CHUP1. (G) Confocal micrographs depict *chup1* KO and FNR control
754 *N. benthamiana* leaf epidermal cells. Four-week-old leaves were infected with tdTomato-
755 expressing *P. infestans*. Imaging was performed 3 days post-inoculation. White arrows indicate
756 haustoria. Yellow and cyan show chloroplast stroma and chloroplast autofluorescence
757 respectively. Scale bars represent 10 µm. (H) Bar graphs demonstrate that the differences in
758 chloroplast-haustoria associations between *chup1* KO plants (44.38%, n = 160 haustoria) and FNR
759 plants (40.17%, n = 229 haustoria) are not significant. Error bars represent standard deviation.
760 Statistical significance was assessed using Fisher's exact test in R. (I-J) Chloroplasts in *chup1* KO
761 plants are clustered around the nucleus. (I) Confocal micrographs depicting nuclei in *chup1* KO
762 and FNR plants transiently expressing NLS:BFP (magenta). Yellow and cyan show chloroplast
763 stroma and chloroplast autofluorescence respectively. Scale bars represent 10 µm. (J)
764 Quantification of chloroplast autofluorescence volume surrounding nuclei, marked by transiently
765 expressed NLS:BFP, in *chup1* KO and FNR plants. *chup1* KO plants (791, n = 89 nuclei) exhibit
766 a significant increase in chloroplast clustering around the nucleus compared to control FNR plants
767 (286, n = 74 nuclei). Crossbars represent the mean. Statistical significance was determined using
768 the Mann-Whitney U test in R. Each data point represents a measurement from a single isolated
769 nucleus. (K) Confocal micrographs depict *chup1* KO and FNR plants where the entire depth of the
770 epidermal layer is shown. Chloroplasts are depicted in cyan colour. (L) Bar graphs demonstrate
771 that the differences in the number of chloroplasts in the epidermal layer between *chup1* KO plants

(253, n = 9 micrographs) and FNR plants (301, n = 0 micrographs) are not significant. Error bars represent standard deviation. Statistical significance was assessed using Student's t-test in R. (M) Bar graphs demonstrate that the differences in the total chlorophyll concentration between *chup1* KO plants (1.6 µg/ml, n = 3 plants) and FNR plants (1.4 µg/ml, n = 3 plants) are not significant. Error bars represent standard deviation. Statistical significance was assessed using Mann-Whitney U test in R.

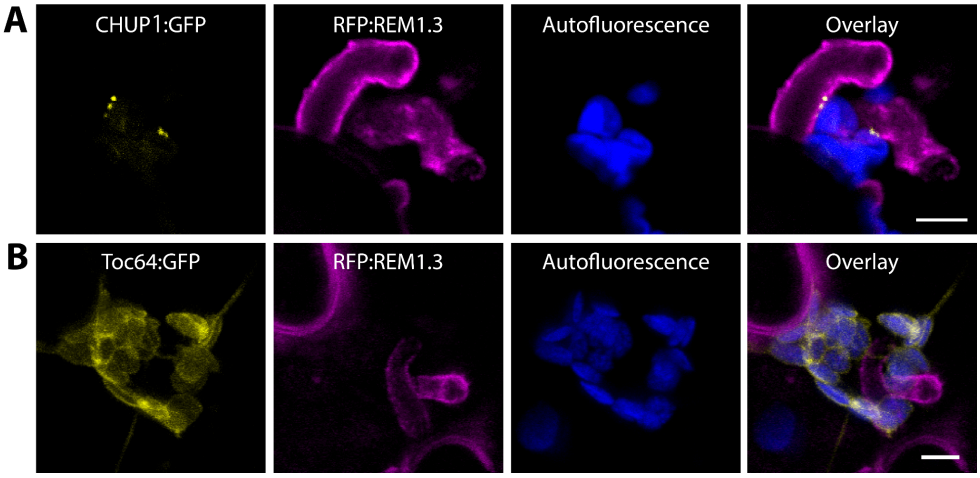

Figure S2. CHUP1 forms punctate accumulation at chloroplast-EHM MCS, but the control Toc64 does not. Additional representative images for Figures 2C and 2D. Confocal micrographs of *N. benthamiana* leaf epidermal cells transiently expressing either (A) CHUP1:GFP, or (B) Toc64:GFP, with RFP:REM1.3. The leaves were infected with WT *P. infestans* spores at 6 hpi. Images were taken at 3 dpi. REM1.3 is used as an EHM marker. Presented images are single plane images. Scale bars represent 5 µm.

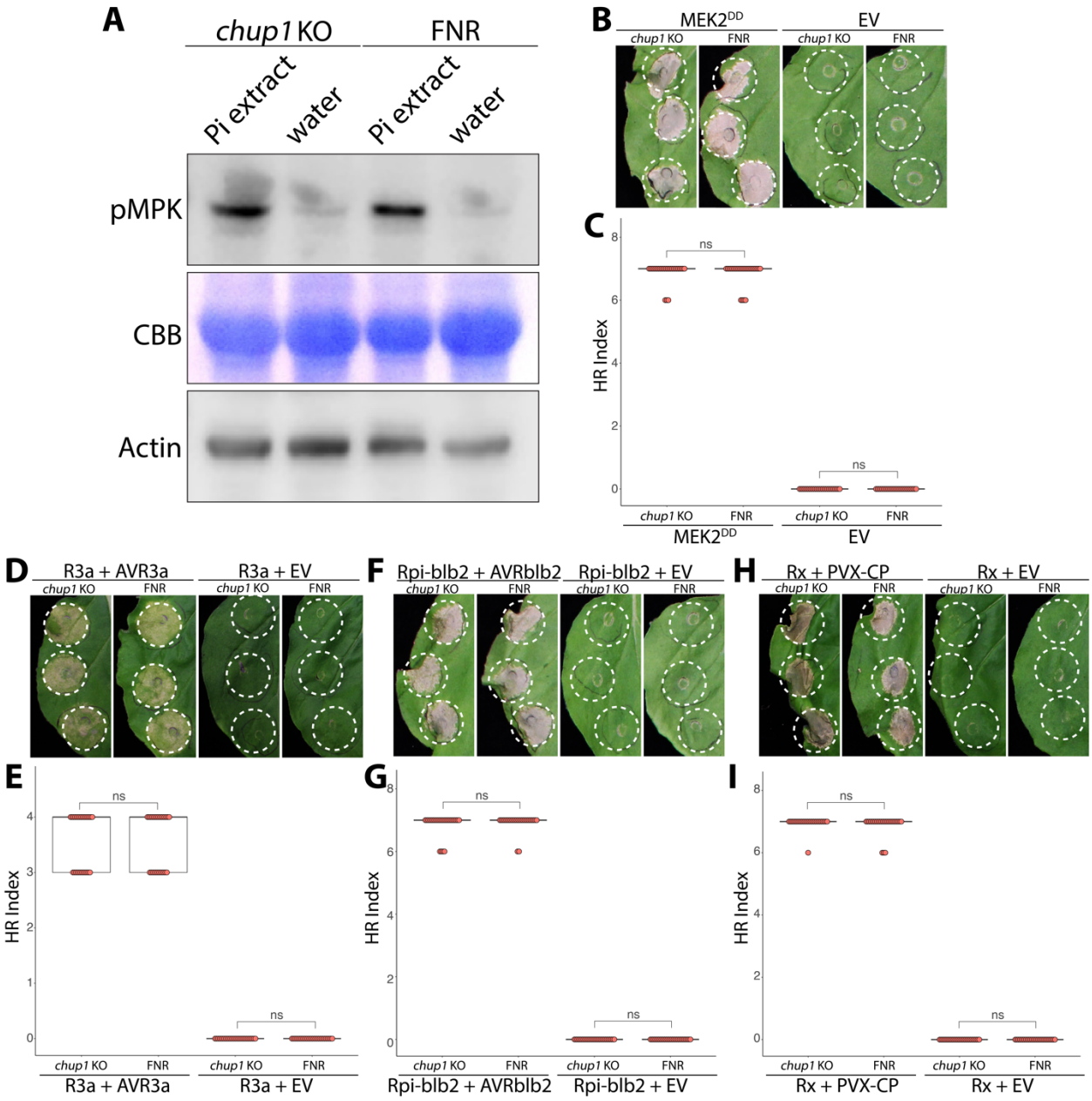

800

801 **Figure S3. The activation of PAMP- or effector-triggered immunity is not impaired in the**

802 **absence of CHUP1.** (A) Western blot analysis of phosphorylated MAPKs in *chup1* KO and FNR

803 plants after a 24-hour treatment with either Pi extract or water. Coomassie brilliant blue staining

804 (CBB) of the gel post protein transfer and actin detection were performed for loading controls. (B-

805 I) For all cell death assays, daylight images were taken, and cell death was scored at 3 dpi.

806 Statistical significance was assessed using Mann-Whitney U test in R. ns = not significant. (B)

807 Representative *chup1* KO and FNR *N. benthamiana* leaves infiltrated with MEK2^{DD} or EV control.
808 (C) Dot plot illustrating that the differences in cell death induced by MEK2^{DD} in *chup1* KO (7, *n*
809 = 27 spots) and FNR plants (7, *n* = 27 spots) are not significant. (D) Representative *chup1* KO and
810 FNR *N. benthamiana* leaves infiltrated with R3a and AVR3a or EV control. (E) Dot plot
811 illustrating that the differences in cell death induced by R3a with AVR3a in *chup1* KO (4, *n* = 27
812 spots) and FNR plants (4, *n* = 27 spots) are not significant. (F) Representative *chup1* KO and FNR
813 *N. benthamiana* leaves infiltrated with Rpi-blb2 and AVRblb2 or EV control. (G) Dot plot
814 illustrating that the differences in cell death induced by Rpi-blb2 with AVRblb2 in *chup1* KO (7,
815 *n* = 27 spots) and FNR plants (7, *n* = 27 spots) are not significant. (H) Representative *chup1* KO
816 and FNR *N. benthamiana* leaves infiltrated with Rx and PVX-CP or EV control. (I) Dot plot
817 illustrating that the differences in cell death induced by Rx with PVX-CP in *chup1* KO (7, *n* = 27
818 spots) and FNR plants (7, *n* = 27 spots) are not significant.

819

820

821

822

823

824

825

826

827

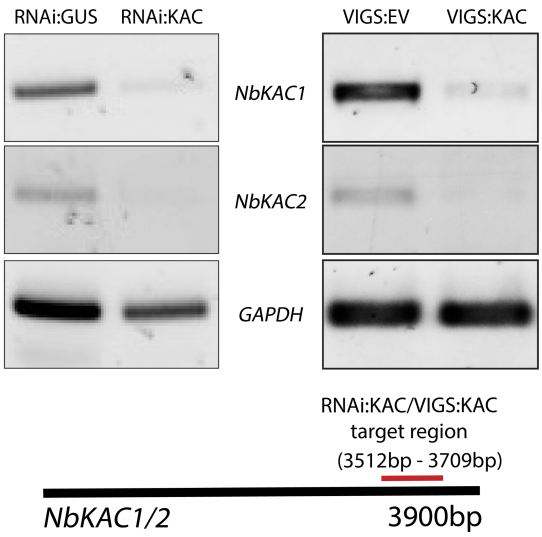

Figure S4. Validation of KAC1 silencing using the RNAi:KAC construct and VIGS:KAC plants. Hairpin plasmids (pRNAi-GG) targeting KAC1 or the GUS reporter gene were infiltrated into *N. benthamiana* leaves. The expression levels of the targeted genes were evaluated via RT-PCR at 3 days post-silencing (left panel). Constructs carrying TRV1 with TRV2-GG targeting *NbKAC1* and *NbKAC2* or the control TRV2:EV were infiltrated into *N. benthamiana leaves*, and the expression levels of the targeted genes were assessed via RT-PCR at 3 weeks post-VIGS (right panel). RT-PCR analysis utilized primers KAC1_RTPCR_F and KAC1_RTPCR_R for *NbKAC1*, and KAC2_RTPCR_F and KAC2_RTPCR_R for *NbKAC2*. The results confirmed gene silencing of *NbKAC1* and *NbKAC2* using the RNAi:KAC construct (left panel) and of the VIGS:KAC plants (right panel). Glyceraldehyde 3-phosphate dehydrogenase (GAPDH) served as the internal control, using primers GAPDH_RTPCR_F and GAPDH_RTPCR_R for assessment. The cDNA was synthesized from total RNA.

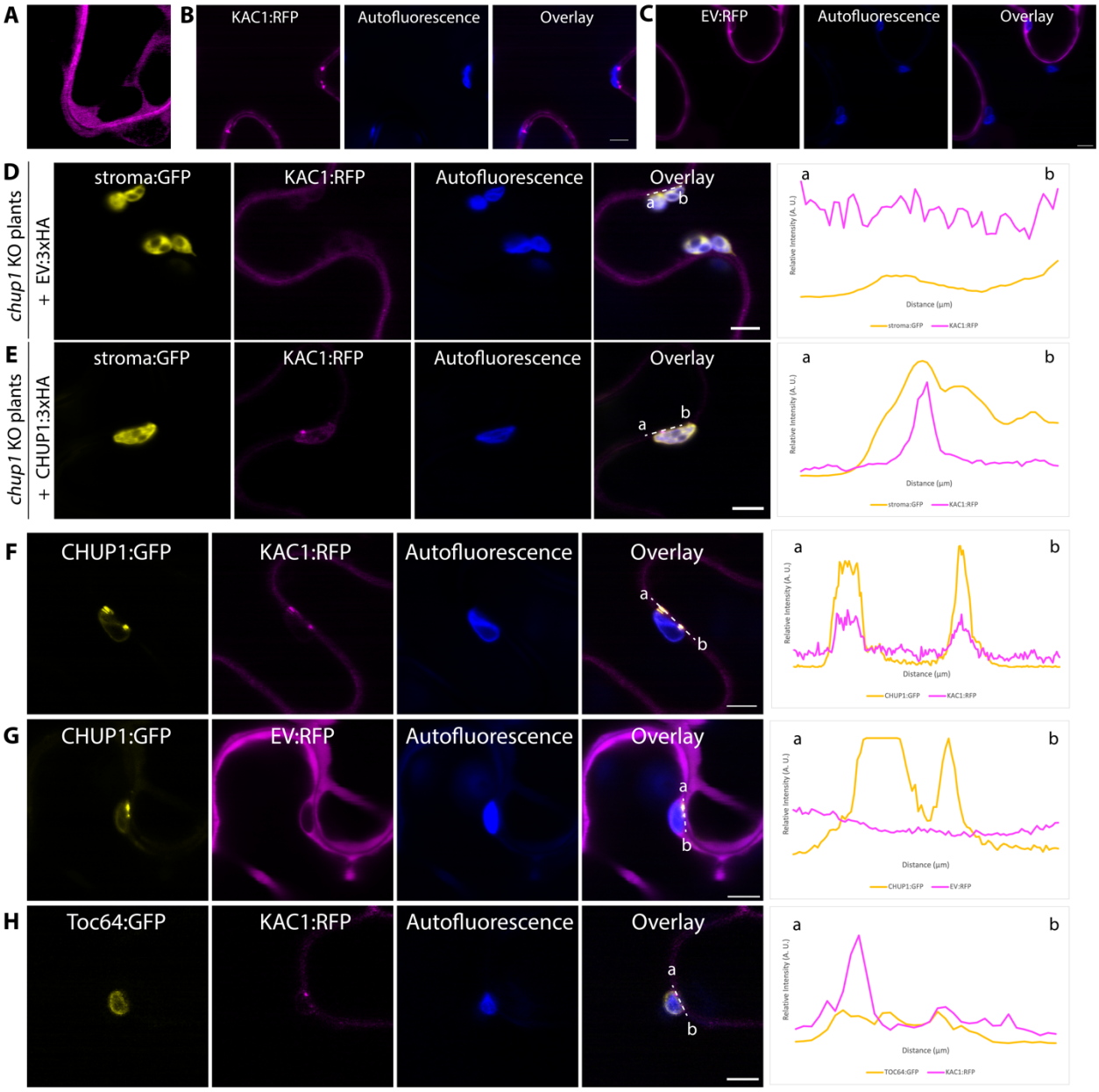

842

843 **Figure S5. KAC1 interacts with CHUP1 and they colocalize at chloroplast-PM MCS.** (A)
844 KAC1:RFP localizes to the PM and cytosol. Confocal micrograph of *N. benthamiana* leaf
845 epidermal cells transiently expressing KAC1:RFP. (B-C) KAC1:RFP forms punctate
846 accumulation at chloroplast-PM MCS, but the control EV:RFP does not. Confocal micrographs of
847 *N. benthamiana* leaf epidermal cells transiently expressing either (B) KAC1:RFP or (C) EV:RFP.
848 (D-E) CHUP1 is required for KAC1 to form punctate structures at chloroplast-PM MCS. Confocal

849 micrographs of *chup1* KO *N. benthamiana* leaf epidermal cells transiently expressing KAC1:RFP
850 with (D) EV:3xHA, or (E) CHUP1:3xHA. GFP channel depicts chloroplast stroma in *chup1* KO
851 plants. (F-H) CHUP1, but not Toc64, colocalizes with KAC1 at punctate structures at chloroplast-
852 PM MCS. Confocal micrographs of *N. benthamiana* leaf epidermal cells transiently expressing (F)
853 CHUP1:GFP and KAC1:RFP, (G) CHUP1:GFP and EV:RFP, and (H) Toc64:GFP and
854 KAC1:RFP. All presented confocal images are single plane images. Images were taken at 3 dpi.
855 Autofluorescence channel depicts chloroplasts. Transects in overlay panels correspond to line
856 intensity plots depicting the relative fluorescence across the marked distance. Scale bars represent
857 5 µm.

858

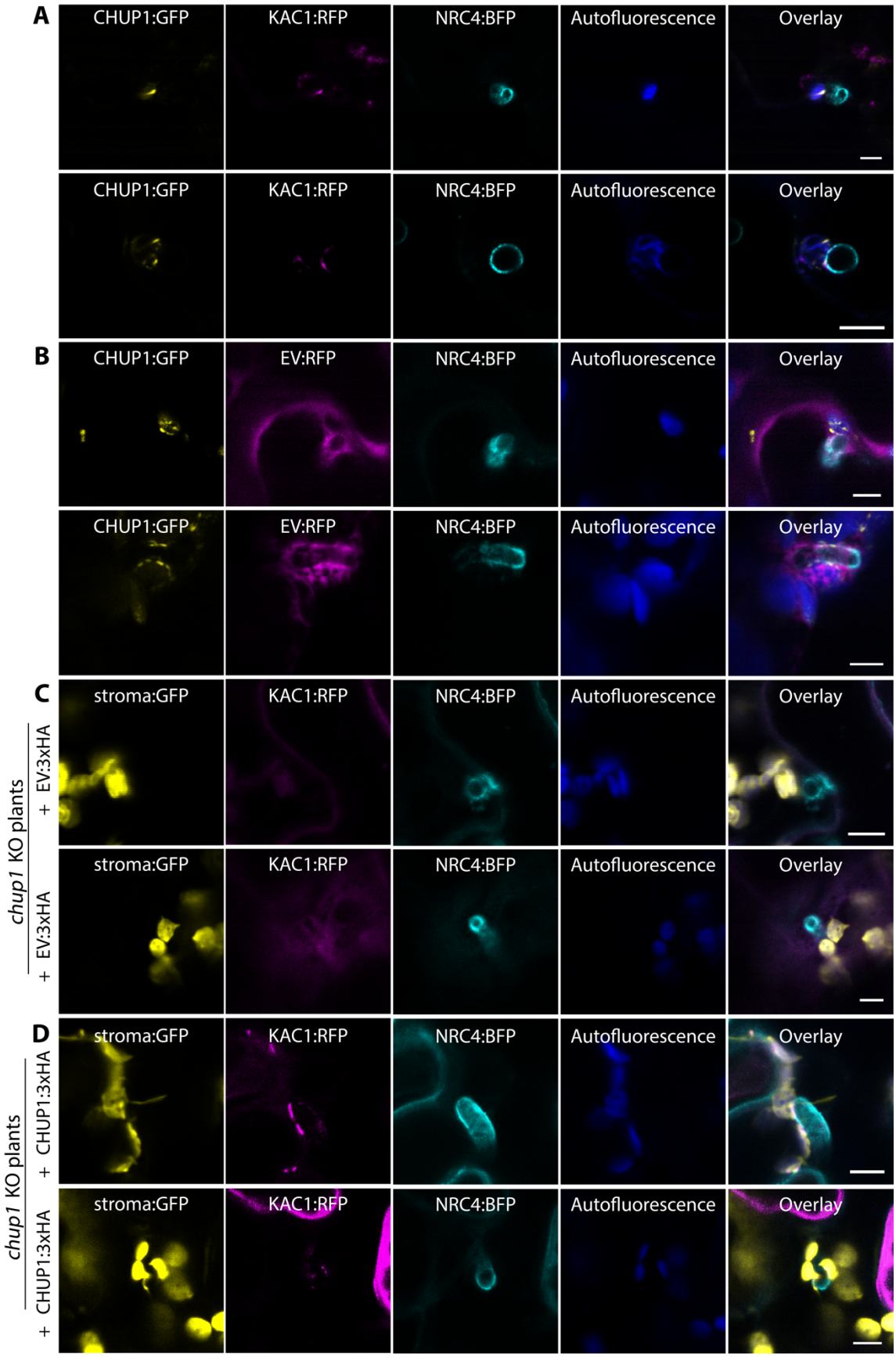
A
CHUP1:GFP
KAC1:RFP
NRC4:BFP
Autofluorescence
Overlay
CHUP1:GFP
KAC1:RFP
NRC4:BFP
Autofluorescence
Overlay
B
CHUP1:GFP
EV:RFP
NRC4:BFP
Autofluorescence
Overlay
CHUP1:GFP
EV:RFP
NRC4:BFP
Autofluorescence
Overlay
C
chup1 KO plants
+ EV:3xHA
stroma:GFP
KAC1:RFP
NRC4:BFP
Autofluorescence
Overlay
+ EV:3xHA
stroma:GFP
KAC1:RFP
NRC4:BFP
Autofluorescence
Overlay
D
chup1 KO plants
+ CHUP1:3xHA
stroma:GFP
KAC1:RFP
NRC4:BFP
Autofluorescence
Overlay
+ CHUP1:3xHA
stroma:GFP
KAC1:RFP
NRC4:BFP
Autofluorescence
Overlay

859

860 **Figure S6. KAC1 colocalizes with CHUP1 at chloroplast-EHM MCS.** Additional
861 representative images for Figures 5A – 5D. (A-B) Additional representative images for Figures
862 5A and 5B. CHUP1 colocalizes with KAC1 at punctate structures at chloroplast-EHM MCS.
863 Confocal micrographs of *N. benthamiana* leaf epidermal cells transiently expressing CHUP1:GFP
864 and NRC4:BFP, with (A) KAC1:RFP, or (B) EV:RFP. NRC4:BFP acts as an EHM marker. The
865 leaves were infected with WT *P. infestans* spores at 6 hpi, and imaged at 3 dpi. (C-D) Additional
866 representative images for Figures 5C and 5D. CHUP1 is required for KAC1 to form punctate
867 structures at chloroplast-EHM MCS. Confocal micrographs of *chup1* KO *N. benthamiana* leaf
868 epidermal cells transiently expressing KAC1:RFP and NRC4:BFP with (C) EV:3xHA, or (D)
869 CHUP1:3xHA. NRC4:BFP acts as an EHM marker. The leaves were infected with WT *P. infestans*
870 spores at 6 hpi, and imaged at 3 dpi. All presented confocal images are single plane images.
871 Autofluorescence channel depicts chloroplasts. GFP channel depicts chloroplast stroma in *chup1*
872 KO plants. Scale bars represent 5 μm.

873

874

875

876

877

878

879

880 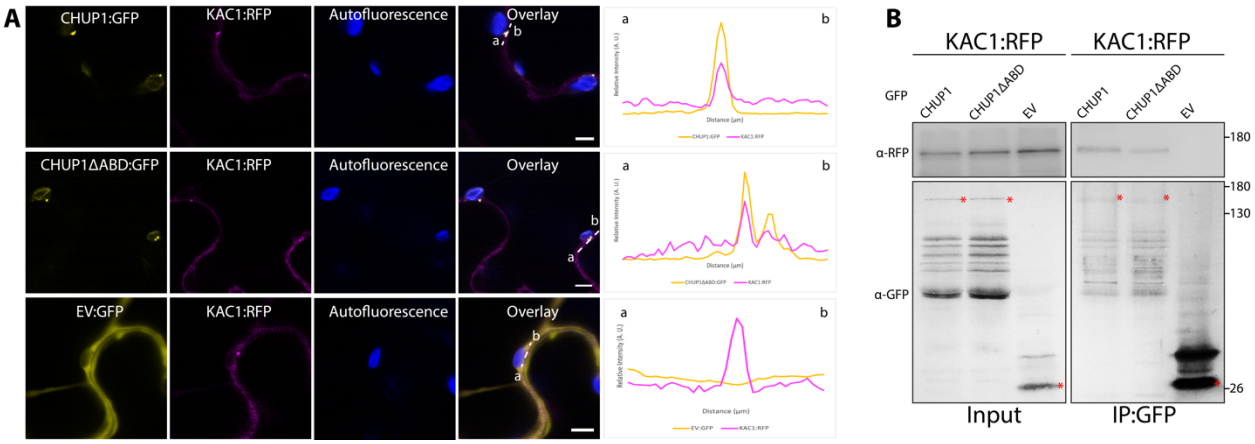

881 **Figure S7. CHUP1 colocalizes and interacts with KAC1 independent of the actin-binding**
882 **domain of CHUP1.** (A) CHUP1 colocalizes with KAC1 at punctate structures at chloroplast-PM
883 MCS independent of its actin-binding domain. Confocal micrographs of *N. benthamiana* leaf
884 epidermal cells transiently expressing CHUP1:GFP and KAC1:RFP (1st row), CHUP1ΔABD:GFP
885 and KAC1:RFP (2nd row), and EV:GFP and KAC1:RFP (3rd row). All presented confocal images
886 are single plane images. Images were taken at 3 dpi. Autofluorescence channel depicts
887 chloroplasts. Transects in overlay panels correspond to line intensity plots depicting the relative
888 fluorescence across the marked distance. Scale bars represent 5 µm. (B) CHUP1 interacts with
889 KAC1 independent of its actin-binding domain. KAC1:RFP was transiently co-expressed with
890 either CHUP1:GFP, CHUP1ΔABD:GFP, or EV:GFP. IPs were obtained with anti-GFP antibody.
891 Total protein extracts were immunoblotted. Red asterisks indicate band sizes. Numbers on the right
892 indicate kDa values.

893

894

895

896 **Table S1. List of primers and synthetic fragment used in this study**

Primer	Sequence
CHUP1_F	CAGGCGGCCGCACTAGTGATGATCGTCAGGGTAGGTTTAGTGG
CHUP1_R	GCAGATCCAGCAGATCCGATTGTTTCTTGTGTATTCTCTTCTCC
CHUP1_sil_F	AGAATGAAATGGTTGCCC
CHUP1_sil_R	GATCCTGCGTATTCTAACATC
NbCHUP1a_RTPCR_F	ATGATCGTCAGGGTAGGTTTAGTGGTTGC
NbCHUP1a_RTPCR_R	TGTTTCTTGTGTATTCTCTTCTCCTGTTTGT
NbCHUP1b_RTPCR_F	TGATAGTCAGGGTAGGTTTAGTGGTTGC
NbCHUP1b_RTPCR_R	TGTTTCTTGTGTATTCTCTTCTCCTGTTTGA
CHUP1Nterm_R	GCAGATCCAGCAGATCCGATGGGTTTTACATTTATCTGCTTAACTGC
CHUP1KO_genotype_F	AGCTTGATCTTGATGATGATCTTTTC
CHUP1KO_genotype_R	TCTTTGTTCTTCCTCTTAAGCTCCA

CHUP1KO2_genotype_F	GTGTGCTTTAGAAACAGTAATTTAAGTC
CHUP1KO2_genotype_R	TCTTTGTTCTTCCTCTTAAGCTCC
CHUP1ΔABD_Frag1_R	CGAAGTTCAAATCTTAAGCATTCAACTTCACTGAATCTGT
CHUP1ΔABD_Frag2_F	ACAGATTCAGTGAAGTTGAATGCTTAAGATTTGAACTTCG
KAC1_F	CAGGCGGCCGCACTAGTGATATGGCGGAGCAGAAGAGC
KAC1_R	GCAGATCCAGCAGATCCGATTGATTTGACATCCTTCAGCAC
KAC1_sil_F	ACCAGGTCTCAGGAGGATTAGGGGGTGAAACTGAC
KAC1_sil_R	ACCAGGTCTCATCGTAGCTCATATTTTCAAGAACG
KAC1_RTPCR_F	GATATCGTTCCATATGCAAATTCAGT
KAC1_RTPCR_R	GTTGAGCTACTTGATTTCTAGTTTGT
KAC2_RTPCR_F	GCTCTAGCCGTGGTAGTAGC
KAC2_RTPCR_R	AACAGATTCTAAAGCTGAACGTAGC
GAPDH_RTPCR_F	ATGGCTTCTCATGCAGCTTT
GAPDH_RTPCR_R	ATCCTGTGGTCTTGGGAGTG
NLS	GGCGGCCGCACTAGTGATGCCTAAAAAGAAGCGTAAGGTTGAGGACCCTGATATCGGATCTGCTGGATCT
Synthetic fragment	**Sequence**

MEK2^{DD}	CAGGCGGCCGCACTAGTGATGCGACCTCTTCAACCACCCC CACCAGCCGCCGCCGCCACCACTACCTCCTCTTCCACCACC GCATCACCCATGCCCCCTCCTCCTTCACGCAACCGTCCCCG TCGTCGTACCAATTTAACTCTCCCCCTTCCCCAACGTGACC CAGCTCTCGCCGTACCCCTCCCCCTCCCCCCTACTTCCGCC CCTTCTTCCTCGTCGTCTTCCTCTTCCTCCCCACTCCCCACC CCCTTAAACTTCTCCGAACTTGAGCGCATCAATCGCATCGG CAGCGGCGCTGGCGGTACGGTTTACAAAGTCCTATATCGC CCCACCGGAAGACTCTACGCTCTCAAAGTCATCTACGGTA ACCACGAGGACTCCGTTCGCCTTCAGATGTGCCGTGAGAT CGAGATTCTCCGTGACGTCGACAACCCTAACGTCGTTAGAT GTCACGATATGTTCGATCACAACGGTGAAATCCAAGTCCT CCTTGAATTCATGGATAAAGGCTCTCTTGAAGGGATCCAC ATCCCTAAAGAGTCAGCTCTTTCGGATCTAACCCGACAAGT CCTCTCGGGACTCTATTATCTCCACAGGCGTAAGATTGTGC ACAGAGATATCAAGCCCTCGAATTTACTAATCAACTCGAG GCGTGAGGTGAAAATTGCTGACTTTGGGGTGTCGAGAGTG CTGGCACAAGACATGGATCCTTGTAATGATTCAGTTGGGA CAATTGCCTATATGAGTCCAGAGAGAATCAACACAGATCT GAATCATGGACAGTACGATGGGTATGCTGGAGATATATGG AGTCTTGGTGTTAGCATATTGGAGTTTTATTTGGGAAGGTT TCCGTTTTCTGTTGGGAGGTCAGGTGATTGGGCTAGTCTTA TGTGCGCCATTTGTATGTCGCAGCCGCCGGAGGCTCCGGC

	GAATGCTTCTAGAGAGTTCAGGGACTTTATTGCTTGCTGTTTGCAGAGGGATCCTGCGCGGCGGTGGACGGCGGTGCAGCTGTTGCGTCATCCATTTATTACCCAGAATAGACCAGCCACTACCACCACCGGTAATATGATGCCACTTCCTAATCAAGTTCATCAGCCAGCACATCAATTGTTACCCCCGCCTCATTTTTCTTCTATCGGATCTGCTGGATCTGC

897

898 **Table S2. List of constructs used in this study**

Construct	Reference
Vector (pK7WGF2 domesticated for Gibson assembly)	[64]
Vector (pRNAI-GG)	[61]
Vector (TRV2-GG)	[60]
TRV1	[65]
TRV2:EV	[60]
TRV2:KAC	This work (primers: KAC1_sil_F and KAC1_sil_R)
TRV2:CHUP1	This work (primers: CHUP1_sil_F and CHUP1_sil_R)
RNAi:KAC	This work (primers: KAC1_sil_F and KAC1_sil_R)
RNAi:GUS	[66]

KAC1:RFP	This work (primers: KAC1_F and KAC1_R)
CHUP1:GFP	This work (primers: CHUP1_F and CHUP1_R)
CHUP1:3xHA	This work (primers: CHUP1_F and CHUP1_R)
CHUP1^{Nterm}:GFP	This work (primers: CHUP1_F and CHUP1Nterm_R)
CHUP1ΔABD:GFP	This work (primers: CHUP1_F and CHUP1ΔABD_Frag1_R, CHUP1ΔABD_Frag2_F and CHUP1_R)
Toc64:GFP	[67]
RFP:REM1.3	[42]
NRC4:BFP	[68]
EV:GFP	[68]
EV:RFP	[59]
3xHA:EV	[69]
NLS:BFP	This work (primer: NLS)
MEK2^{DD}:3xHA	This work (synthetic fragment: MEK2^{DD})
AVR3a	Provided by TSLSynBio
R3a	[70]
GFP:AVRblb2	[1]
RFP:Rpi-blb2	[1]
PVX-CP	[71]
Rx	[71]

899

900 **References**

901

902 1 Bozkurt, T. O. *et al.* Phytophthora infestans effector AVRblb2 prevents secretion of a plant
903 immune protease at the haustorial interface. *Proceedings of the National Academy of*
904 *Sciences* **108**, 20832-20837 (2011).
905 2 Kwon, C. *et al.* Co-option of a default secretory pathway for plant immune responses.
906 *Nature* **451**, 835-840 (2008).
907 3 Yuen, E. L. H. *et al.* A RabGAP negatively regulates plant autophagy and immune
908 trafficking. *Current Biology* (2024).
909 4 Yuen, E. L. H., Shepherd, S. & Bozkurt, T. O. Traffic Control: Subversion of Plant
910 Membrane Trafficking by Pathogens. *Annual Review of Phytopathology* **61** (2023).
911 5 Bozkurt, T. O. & Kamoun, S. The plant–pathogen haustorial interface at a glance. *Journal*
912 *of Cell Science* **133**, jcs237958 (2020).
913 6 Heath, M. C., Nimchuk, Z. L. & Xu, H. Plant nuclear migrations as indicators of critical
914 interactions between resistant or susceptible cowpea epidermal cells and invasion hyphae
915 of the cowpea rust fungus. *The New Phytologist* **135**, 689-700 (1997).
916 7 Savage, Z. *et al.* Chloroplasts alter their morphology and accumulate at the pathogen
917 interface during infection by Phytophthora infestans. *The Plant Journal* **107**, 1771-1787
918 (2021).
919 8 Fuchs, R. *et al.* Immobilized subpopulations of leaf epidermal mitochondria mediate
920 PENETRATION2-dependent pathogen entry control in Arabidopsis. *The Plant Cell* **28**,
921 130-145 (2016).
922 9 Chung, J. *et al.* PI4P/phosphatidylserine countertransport at ORP5-and ORP8-mediated
923 ER–plasma membrane contacts. *Science* **349**, 428-432 (2015).
924 10 Prinz, W. A., Toulmay, A. & Balla, T. The functional universe of membrane contact sites.
925 *Nature reviews Molecular cell biology* **21**, 7-24 (2020).
926 11 Pérez-Sancho, J. *et al.* Stitching organelles: organization and function of specialized
927 membrane contact sites in plants. *Trends in Cell Biology* **26**, 705-717 (2016).

928 12 Hubber, A. *et al.* The machinery at endoplasmic reticulum-plasma membrane contact sites
929 contributes to spatial regulation of multiple Legionella effector proteins. *PLoS pathogens*
930 **10**, e1004222 (2014).
931 13 Agaisse, H. & Derré, I. Expression of the effector protein IncD in Chlamydia trachomatis
932 mediates recruitment of the lipid transfer protein CERT and the endoplasmic reticulum-
933 resident protein VAPB to the inclusion membrane. *Infection and immunity* **82**, 2037-2047
934 (2014).
935 14 Vormittag, S., Ende, R. J., Derré, I. & Hilbi, H. Pathogen vacuole membrane contact sites–
936 close encounters of the fifth kind. *Microlife* **4**, uqad018 (2023).
937 15 Littlejohn, G. R., Breen, S., Smirnoff, N. & Grant, M. Chloroplast immunity illuminated.
938 *New Phytologist* **229**, 3088-3107 (2021).
939 16 Nomura, H. *et al.* Chloroplast-mediated activation of plant immune signalling in
940 Arabidopsis. *Nature communications* **3**, 926 (2012).
941 17 Su, J. *et al.* Active photosynthetic inhibition mediated by MPK3/MPK6 is critical to
942 effector-triggered immunity. *PLoS Biology* **16**, e2004122 (2018).
943 18 Caplan, J. L. *et al.* Chloroplast stromules function during innate immunity. *Developmental*
944 *cell* **34**, 45-57 (2015).
945 19 Jung, S., Woo, J. & Park, E. Talk to your neighbors in an emergency: Stromule-mediated
946 chloroplast-nucleus communication in plant immunity. *Current Opinion in Plant Biology*
947 **79**, 102529 (2024).
948 20 Ding, X., Jimenez-Gongora, T., Krenz, B. & Lozano-Duran, R. Chloroplast clustering
949 around the nucleus is a general response to pathogen perception in Nicotiana benthamiana.
950 *Molecular plant pathology* **20**, 1298-1306 (2019).
951 21 de Torres Zabala, M. *et al.* Chloroplasts play a central role in plant defence and are targeted
952 by pathogen effectors. *Nature plants* **1**, 1-10 (2015).
953 22 Gao, C. *et al.* Pathogen manipulation of chloroplast function triggers a light-dependent
954 immune recognition. *Proceedings of the National Academy of Sciences* **117**, 9613-9620
955 (2020).
956 23 Jelenska, J. *et al.* AJ domain virulence effector of Pseudomonas syringae remodels host
957 chloroplasts and suppresses defenses. *Current Biology* **17**, 499-508 (2007).

958 24 Pecrix, Y. *et al.* Sunflower resistance to multiple downy mildew pathotypes revealed by
959 recognition of conserved effectors of the oomycete Plasmopara halstedii. *The Plant*
960 *Journal* **97**, 730-748 (2019).
961 25 Petre, B. *et al.* Rust fungal effectors mimic host transit peptides to translocate into
962 chloroplasts. *Cellular microbiology* **18**, 453-465 (2016).
963 26 Xu, Q. *et al.* An effector protein of the wheat stripe rust fungus targets chloroplasts and
964 suppresses chloroplast function. *Nature Communications* **10**, 5571 (2019).
965 27 Shepherd, S., Yuen, E. L. H., Carella, P. & Bozkurt, T. O. The wheels of destruction: Plant
966 NLR immune receptors are mobile and structurally dynamic disease resistance proteins.
967 *Current Opinion in Plant Biology* **74**, 102372 (2023).
968 28 King, F. J., Yuen, E. L. H. & Bozkurt, T. O. Border control: Manipulation of the host–
969 pathogen interface by perihaustorial oomycete effectors. *Molecular Plant-Microbe*
970 *Interactions* **37**, 220-226 (2024).
971 29 Wang, S. *et al.* The Phytophthora infestans haustorium is a site for secretion of diverse
972 classes of infection-associated proteins. *MBio* **9**, 10.1128/mbio. 01216-01218 (2018).
973 30 Whisson, S. C. *et al.* A translocation signal for delivery of oomycete effector proteins into
974 host plant cells. *Nature* **450**, 115-118 (2007).
975 31 Oikawa, K. *et al.* Chloroplast unusual positioning1 is essential for proper chloroplast
976 positioning. *The Plant Cell* **15**, 2805-2815 (2003).
977 32 Oikawa, K. *et al.* Chloroplast outer envelope protein CHUP1 is essential for chloroplast
978 anchorage to the plasma membrane and chloroplast movement. *Plant physiology* **148**, 829-
979 842 (2008).
980 33 Suetsugu, N. *et al.* The KAC family of kinesin-like proteins is essential for the association
981 of chloroplasts with the plasma membrane in land plants. *Plant and cell physiology* **53**,
982 1854-1865 (2012).
983 34 Suetsugu, N. *et al.* Two kinesin-like proteins mediate actin-based chloroplast movement in
984 Arabidopsis thaliana. *Proceedings of the National Academy of Sciences* **107**, 8860-8865
985 (2010).
986 35 Kadota, A. *et al.* Short actin-based mechanism for light-directed chloroplast movement in
987 Arabidopsis. *Proceedings of the National Academy of Sciences* **106**, 13106-13111 (2009).

988 36 Irieda, H. & Takano, Y. Epidermal chloroplasts are defense-related motile organelles
989 equipped with plant immune components. *Nature communications* **12**, 2739 (2021).
990 37 Schmidt von Braun, S. & Schleiff, E. The chloroplast outer membrane protein CHUP1
991 interacts with actin and profilin. *Planta* **227**, 1151-1159 (2008).
992 38 Wada, M. & Kong, S.-G. Actin-mediated movement of chloroplasts. *Journal of Cell*
993 *Science* **131**, jcs210310 (2018).
994 39 Sohrt, K. & Soll, J. Toc64, a new component of the protein translocon of chloroplasts. *The*
995 *Journal of cell biology* **148**, 1213-1222 (2000).
996 40 Koh, S., André, A., Edwards, H., Ehrhardt, D. & Somerville, S. Arabidopsis thaliana
997 subcellular responses to compatible Erysiphe cichoracearum infections. *The Plant Journal*
998 **44**, 516-529 (2005).
999 41 Micali, C. O., Neumann, U., Grunewald, D., Panstruga, R. & O'Connell, R. Biogenesis of
1000 a specialized plant–fungal interface during host cell internalization of Golovinomyces
1001 orontii haustoria. *Cellular microbiology* **13**, 210-226 (2011).
1002 42 Bozkurt, T. O. *et al.* The plant membrane-associated REMORIN1. 3 accumulates in
1003 discrete perihaustorial domains and enhances susceptibility to Phytophthora infestans.
1004 *Plant physiology* **165**, 1005-1018 (2014).
1005 43 Yang, K.-Y., Liu, Y. & Zhang, S. Activation of a mitogen-activated protein kinase pathway
1006 is involved in disease resistance in tobacco. *Proceedings of the national academy of*
1007 *sciences* **98**, 741-746 (2001).
1008 44 Bos, J. I. *et al.* The C-terminal half of Phytophthora infestans RXLR effector AVR3a is
1009 sufficient to trigger R3a-mediated hypersensitivity and suppress INF1-induced cell death
1010 in Nicotiana benthamiana. *The Plant Journal* **48**, 165-176 (2006).
1011 45 Oh, S.-K. *et al.* In planta expression screens of Phytophthora infestans RXLR effectors
1012 reveal diverse phenotypes, including activation of the Solanum bulbocastanum disease
1013 resistance protein Rpi-blb2. *The Plant Cell* **21**, 2928-2947 (2009).
1014 46 Bendahmane, A., Köhm, B. A., Dedi, C. & Baulcombe, D. C. The coat protein of potato
1015 virus X is a strain-specific elicitor of Rx1-mediated virus resistance in potato. *The Plant*
1016 *Journal* **8**, 933-941 (1995).

1017 47 Suetsugu, N., Higa, T., Gotoh, E. & Wada, M. Light-induced movements of chloroplasts
1018 and nuclei are regulated in both cp-actin-filament-dependent and-independent manners in
1019 Arabidopsis thaliana. *PLoS One* **11**, e0157429 (2016).
1020 48 Shen, Z. *et al.* The kinesin-like proteins, KAC1/2, regulate actin dynamics underlying
1021 chloroplast light-avoidance in Physcomitrella patens. *Journal of integrative plant biology*
1022 **57**, 106-119 (2015).
1023 49 Singh, R. *et al.* Two chloroplast-localized proteins: AtNHR2A and AtNHR2B, contribute
1024 to callose deposition during nonhost disease resistance in Arabidopsis. *Molecular Plant-*
1025 *Microbe Interactions* **31**, 1280-1290 (2018).
1026 50 Cheval, C. *et al.* Chitin perception in plasmodesmata characterizes submembrane immune-
1027 signaling specificity in plants. *Proceedings of the National Academy of Sciences* **117**, 9621-
1028 9629 (2020).
1029 51 Castro, B. *et al.* Stress-induced reactive oxygen species compartmentalization, perception
1030 and signalling. *Nature plants* **7**, 403-412 (2021).
1031 52 Almagro, L. *et al.* Class III peroxidases in plant defence reactions. *Journal of experimental*
1032 *botany* **60**, 377-390 (2009).
1033 53 Kong, S.-G. *et al.* CHLOROPLAST UNUSUAL POSITIONING 1 is a plant-specific actin
1034 polymerization factor regulating chloroplast movement. *The Plant Cell* **36**, 1159-1181
1035 (2024).
1036 54 Jeong, R.-D., Kachroo, A. & Kachroo, P. Blue light photoreceptors are required for the
1037 stability and function of a resistance protein mediating viral defense in Arabidopsis. *Plant*
1038 *signaling & behavior* **5**, 1504-1509 (2010).
1039 55 Naqvi, S. *et al.* Blue-light receptor phototropin 1 suppresses immunity to promote
1040 Phytophthora infestans infection. *New Phytologist* **233**, 2282-2293 (2022).
1041 56 Erickson, J. L., Kantek, M. & Schattat, M. H. Plastid-nucleus distance alters the behavior
1042 of stromules. *Frontiers in Plant Science* **8**, 265203 (2017).
1043 57 Stuttmann, J. *et al.* Highly efficient multiplex editing: one-shot generation of 8× Nicotiana
1044 benthamiana and 12× Arabidopsis mutants. *The Plant Journal* **106**, 8-22 (2021).
1045 58 Schattat, M., Barton, K., Baudisch, B., Klösgen, R. B. & Mathur, J. Plastid stromule
1046 branching coincides with contiguous endoplasmic reticulum dynamics. *Plant physiology*
1047 **155**, 1667-1677 (2011).

1048 59 Dagdas, Y. F. *et al.* An effector of the Irish potato famine pathogen antagonizes a host
1049 autophagy cargo receptor. *Elife* **5**, e10856 (2016).
1050 60 Duggan, C. A golden-gate compatible TRV2 virus induced gene silencing (VIGS) vector.
1051 *Zenodo* (2021).
1052 61 Yan, P. *et al.* High-throughput construction of intron-containing hairpin RNA vectors for
1053 RNAi in plants. *PLOS one* **7**, e38186 (2012).
1054 62 Wellburn, A. R. The spectral determination of chlorophylls a and b, as well as total
1055 carotenoids, using various solvents with spectrophotometers of different resolution.
1056 *Journal of plant physiology* **144**, 307-313 (1994).
1057 63 Wu, C.-H. *et al.* NLR network mediates immunity to diverse plant pathogens. *Proceedings*
1058 *of the National Academy of Sciences* **114**, 8113-8118 (2017).
1059 64 Dagdas, Y. F. *et al.* Host autophagy machinery is diverted to the pathogen interface to
1060 mediate focal defense responses against the Irish potato famine pathogen. *Elife* **7**, e37476
1061 (2018).
1062 65 Ratcliff, F., Martin-Hernandez, A. M. & Baulcombe, D. C. Technical advance: tobacco
1063 rattle virus as a vector for analysis of gene function by silencing. *The Plant Journal* **25**,
1064 237-245 (2001).
1065 66 Yuen, E. L. H. *et al.* An oomycete effector co-opts a host RabGAP protein to remodel
1066 pathogen interface and subvert defense-related secretion. *bioRxiv*, 2024.2001.
1067 2011.575225 (2024).
1068 67 Breuers, F. K. *et al.* Dynamic remodeling of the plastid envelope membranes–a tool for
1069 chloroplast envelope in vivo localizations. *Frontiers in plant science* **3**, 17957 (2012).
1070 68 Duggan, C. *et al.* Dynamic localization of a helper NLR at the plant–pathogen interface
1071 underpins pathogen recognition. *Proceedings of the National Academy of Sciences* **118**,
1072 e2104997118 (2021).
1073 69 Pandey, P. *et al.* An oomycete effector subverts host vesicle trafficking to channel
1074 starvation-induced autophagy to the pathogen interface. *Elife* **10**, e65285 (2021).
1075 70 Chaparro-Garcia, A. *et al.* Phytophthora infestans RXLR-WY effector AVR3a associates
1076 with dynamin-related protein 2 required for endocytosis of the plant pattern recognition
1077 receptor FLS2. *PLoS One* **10**, e0137071 (2015).

71 Contreras, M. P. *et al.* Resurrection of plant disease resistance proteins via helper NLR bioengineering. *Science Advances* **9**, eadg3861 (2023).